Thermodynamics of Heisenberg ferromagnets with arbitrary spin in a magnetic field

I. Juhász Junger,[1] D. Ihle,[1] L. Bogacz,[1,2] and W. Janke[1,3]
[1]*Institut für Theoretische Physik, Universität Leipzig, D-04109 Leipzig, Germany*
[2]*Department of Information Technologies, Faculty of Physics, Astronomy and Applied Informatics, Jagellonian University, 30-059 Kraków, Poland*
[3]*Centre for Theoretical Sciences (NTZ), Universität Leipzig, D-04105 Leipzig, Germany*
(Received 21 February 2006; revised manuscript received 20 February 2008; published 8 May 2008)

The thermodynamic properties (magnetization, magnetic susceptibility, transverse and longitudinal correlation lengths, and specific heat) of one- and two-dimensional ferromagnets with arbitrary spin S in a magnetic field are investigated by a second-order Green-function theory. In addition, quantum Monte Carlo simulations for $S=1/2$ and $S=1$ are performed by using the stochastic series expansion method. Good agreement between the results of both approaches is found. The field dependence of the position of the maximum in the temperature dependence of the susceptibility fits well to a power law at low fields and to a linear increase at high fields. The maximum height decreases according to a power law in the whole field region. The longitudinal correlation length may show an anomalous temperature dependence: a minimum followed by a maximum with increasing temperature. Considering the specific heat in one dimension and at low magnetic fields, two maxima in its temperature dependence for both the $S=1/2$ and $S=1$ ferromagnets are found. For $S>1$, only one maximum occurs, as in the two-dimensional ferromagnets. Relating the theory to experiments on the $S=1/2$ quasi-one-dimensional copper salt TMCuC $[(CH_3)_4NCuCl_3]$, a fit to the magnetization as a function of the magnetic field yields the value of the exchange energy, which is used to make predictions for the occurrence of two maxima in the temperature dependence of the specific heat.

DOI: 10.1103/PhysRevB.77.174411 PACS number(s): 75.10.Jm, 75.40.Cx

I. INTRODUCTION

The study of low-dimensional quantum spin systems[1] is of growing interest and is motivated by the progress in the synthesis of new materials, where ferromagnetic compounds attract increasing attention. For example, besides the spin $S=1/2$ quasi-one-dimensional (1D) ferromagnetic systems, such as the copper salt TMCuC,[2,3] the organic magnets *p*-NPNN $(C_{13}H_{16}N_3O_4)$[4,5] and *β*-BBDTA(benzo[1,2-*d*:4,5-*d'*]bis[1,3,2]dithiazole)·GaBr4,[6] and the $CuCl_2$-sulfoxide complexes,[7] recently the $S=1/2$ quasi-two-dimensional (2D) ferromagnet Cs_2AgF_4, which has a structure similar to the high-T_c parent compound La_2CuO_4, was studied[8] and found to be magnetically reminiscent of K_2CuF_4.[9] In ferromagnetic systems with $S\geqslant 1$, mainly the effects of single-ion spin anisotropies were investigated, such as in the quasi-1D $S=1$ easy-plane ferromagnet $CsNiF_3$ (Ref. 10) and in 2D easy-axis Heisenberg models in a magnetic field[11–13] for describing the spin reorientation transition in thin ferromagnetic films (see Ref. 14 and references therein).

The 2D anisotropic $S\geqslant 1$ Heisenberg ferromagnets in a magnetic field were investigated by Green-function methods,[11,13,15] where the exchange term was treated in the random-phase approximation (RPA),[16] and by quantum Monte Carlo (QMC) simulations.[12] In a previous paper,[17] we have developed a second-order Green-function theory of 1D and 2D $S=1/2$ ferromagnets in a magnetic field, which goes one step beyond the RPA and provides a rather good description of magnetic short-range order (SRO) and of the thermodynamics. This can be seen from the comparison to the exact calculations by the Bethe-ansatz method for the quantum transfer matrix in the 1D model and to the exact diagonalizations on finite lattices. In particular, for the $S=1/2$ ferromagnetic chain, two maxima in the temperature dependence of the specific heat at very low magnetic fields were found. On the contrary, the RPA was shown to fail in describing the SRO, reflected, e.g., in the specific heat, whereas the magnetization and the magnetic susceptibility are quite well reproduced. Recently, a similar Green-function approach for $S=1/2$ ferromagnets was presented,[18] which improves the theory of Ref. 17 concerning the agreement with exact methods. The results that are obtained for $S=1/2$ are stimulating to investigate ferromagnets with $S>1/2$ in a magnetic field, for which a second-order Green-function theory of SRO is not developed yet. Second-order Green-function approaches for ferromagnets with arbitrary spin exist in the case of zero magnetic field only,[19,20] where in Ref. 20, ferromagnetic chains with an easy-axis single-ion anisotropy were studied.

In this paper, we extend both our previous theory for $S=1/2$ (Ref. 17) to arbitrary spins and the theory of Ref. 19 for zero field to arbitrary fields. We start from the ferromagnetic Heisenberg model with arbitrary spin S,

$$H=-J\sum_{\langle ij\rangle}\boldsymbol{S}_i\boldsymbol{S}_j-h\sum_i S_i^z \tag{1}$$

[$\langle ij\rangle$ denote the nearest-neighbor (NN) bonds along a chain or on a square lattice; throughout, we set $J=1$], with $\boldsymbol{S}_i^2=S(S+1)$. We calculate thermodynamic properties (magnetization, magnetic susceptibility, correlation length, and specific heat) at arbitrary temperatures and fields. For comparison, we perform QMC simulations of the $S=1/2$ and $S=1$ models on a chain up to $N=L=1024$ sites and on a square lattice up to $N=L\times L=64\times 64$.

The rest of the paper is organized as follows: In Sec. II, the second-order Green-function theory for model (1) is de-

veloped, where the extensions of previous second-order Green-function approaches[17–19] to arbitrary spins and fields imply novel technical aspects. Moreover, considering the case $S=1/2$, the theory is extended as compared to Refs. 17 and 18 by the introduction of two additional vertex parameters and, correspondingly, by taking into consideration two additional conditions for their determination. This extension is shown to have qualitative effects on the temperature dependence of the longitudinal correlation length (see Sec. IV B). In Sec. III, the employed QMC method is briefly described. In Sec. IV, the thermodynamic properties of the 1D and 2D ferromagnets are investigated as functions of temperature and field, also in comparison to RPA, and are related to experiments. Particular attention is paid to the calculation of the transverse and longitudinal correlation lengths, which were not considered in Refs. 17 and 18. Finally, a summary of our work is given in Sec. V.

II. SECOND-ORDER GREEN-FUNCTION THEORY

To determine the transverse and longitudinal spin correlation functions and the thermodynamic quantities, we employ the equation of motion method for two-time retarded commutator Green functions.[16] First, we calculate the transverse spin correlation functions. Because we treat arbitrary spins in nonzero magnetic fields, so that we have $\langle S^z\rangle \neq 0$, we consider the Green functions $\langle\langle S_{\boldsymbol{q}}^+;S_{-\boldsymbol{q}}^{(n)-}\rangle\rangle_\omega$ that were introduced by Tyablikov[16] within the first-order theory, i.e., the RPA (see Appendix), where $S_{-\boldsymbol{q}}^{(n)-}$ is the Fourier transform of $S_i^{(n)-}=(S_i^z)^nS_i^-$ with $n=0,1,\ldots,2S-1$, and the Green functions $\langle\langle i\dot{S}_{\boldsymbol{q}}^+;S_{-\boldsymbol{q}}^{(n)-}\rangle\rangle_\omega$, which we calculate for the first time in the second-order theory. The equations of motion read

$$\omega\langle\langle S_{\boldsymbol{q}}^+;S_{-\boldsymbol{q}}^{(n)-}\rangle\rangle_\omega = M^{(n)+-} + \langle\langle i\dot{S}_{\boldsymbol{q}}^+;S_{-\boldsymbol{q}}^{(n)-}\rangle\rangle_\omega, \tag{2}$$

$$\omega\langle\langle i\dot{S}_{\boldsymbol{q}}^+;S_{-\boldsymbol{q}}^{(n)-}\rangle\rangle_\omega = \tilde{M}_{\boldsymbol{q}}^{(n)+-} + \langle\langle -\ddot{S}_{\boldsymbol{q}}^+;S_{-\boldsymbol{q}}^{(n)-}\rangle\rangle_\omega. \tag{3}$$

The moments $M^{(n)+-}=\langle[S_{\boldsymbol{q}}^+,S_{-\boldsymbol{q}}^{(n)-}]\rangle$ and $\tilde{M}_{\boldsymbol{q}}^{(n)+-}=\langle[i\dot{S}_{\boldsymbol{q}}^+,S_{-\boldsymbol{q}}^{(n)-}]\rangle$ are given by the exact expressions,

$$M^{(n)+-} = 2\langle(S^z)^{n+1}\rangle + (1-\delta_{n,0})\sum_{k=1}^{n}\binom{n}{k}(-1)^k\{S(S+1)\times\langle(S^z)^{n-k}\rangle + \langle(S^z)^{n-k+1}\rangle - \langle(S^z)^{n-k+2}\rangle\}, \tag{4}$$

$$\tilde{M}_{\boldsymbol{q}}^{(n)+-} = z(1-\gamma_{\boldsymbol{q}})\Bigg\{2C_{10}^{(n)zz} + C_{10}^{(n)-+} + (1-\delta_{n,0})\sum_{k=1}^{n}\binom{n}{k}(-1)^k \times[S(S+1)(\delta_{k,n}\langle S^z\rangle + (1-\delta_{k,n})C_{10}^{(n-k-1)zz}) + C_{10}^{(n-k)zz} - C_{10}^{(n-k+1)zz}]\Bigg\} + hM^{(n)+-}, \tag{5}$$

where $C_{nm}^{(n)-+}\equiv C_{\boldsymbol{R}}^{(n)-+}=\langle S_0^{(n)-}S_{\boldsymbol{R}}^+\rangle$, $C_{nm}^{(n)zz}\equiv C_{\boldsymbol{R}}^{(n)zz}=\langle(S_0^z)^{n+1}S_{\boldsymbol{R}}^z\rangle$, $\boldsymbol{R}=n\boldsymbol{e}_x+m\boldsymbol{e}_y$, $\gamma_{\boldsymbol{q}}=\frac{2}{z}\sum_{i=1}^{z/2}\cos q_i$, and z is the coordination number. Deriving Eqs. (4) and (5), the operator identity

$$\boldsymbol{S}_i^2 = S_i^-S_i^+ + S_i^z + (S_i^z)^2 \tag{6}$$

has been used. In Eq. (3), the second derivative $-\ddot{S}_{\boldsymbol{q}}^+$ is approximated as indicated in Refs. 17 and 19–24. That means, in $-\ddot{S}_i^+$, we decouple the products of operators along NN sequences $\langle i,j,l\rangle$ as

$$S_i^+S_j^+S_l^- = \alpha_1^{+-}\langle S_j^+S_l^-\rangle S_i^+ + \alpha_2^{+-}\langle S_i^+S_l^-\rangle S_j^+, \tag{7}$$

where the vertex parameters α_1^{+-} and α_2^{+-} are attached to NN and further-distant correlation functions, respectively. The products of operators with two coinciding sites, appearing for $S\geqslant 1$, are decoupled as[19,20]

$$S_i^+S_j^-S_j^+ = \langle S_j^-S_j^+\rangle S_i^+ + \lambda^{+-}\langle S_i^+S_j^-\rangle S_j^+, \tag{8}$$

where the vertex parameter λ^{+-} is introduced. We obtain

$$-\ddot{S}_{\boldsymbol{q}}^+ = [(\omega_{\boldsymbol{q}}^{+-})^2 - h^2]S_{\boldsymbol{q}}^+ + 2hi\dot{S}_{\boldsymbol{q}}^+, \tag{9}$$

with

$$(\omega_{\boldsymbol{q}}^{+-})^2 = \frac{z}{2}(1-\gamma_{\boldsymbol{q}})\{\Delta^{+-} + 2z\alpha_1^{+-}C_{10}(1-\gamma_{\boldsymbol{q}})\}, \tag{10}$$

$$\Delta^{+-} = S(S+1) + \langle(S^z)^2\rangle + 2\{\lambda^{+-} - (z+1)\alpha_1^{+-}\}C_{10} + 2\alpha_2^{+-}\{(z-2)C_{11} + C_{20}\}, \tag{11}$$

where $C_{nm}=\frac{1}{2}C_{nm}^{(0)-+}+C_{nm}^{(0)zz}$. In the special case $S=1/2$, in $-\ddot{S}_i^+$, products of spin operators with two coinciding sites do not appear, which is equivalent to setting $\lambda^{+-}=0$. Finally, we get the Green functions,

$$\langle\langle S_{\boldsymbol{q}}^+;S_{-\boldsymbol{q}}^{(n)-}\rangle\rangle_\omega = \sum_{i=1,2}\frac{A_{\boldsymbol{q}i}^{(n)}}{\omega-\omega_{\boldsymbol{q}i}}, \tag{12}$$

$$\langle\langle i\dot{S}_{\boldsymbol{q}}^+;S_{-\boldsymbol{q}}^{(n)-}\rangle\rangle_\omega = \sum_{i=1,2}\frac{\omega_{\boldsymbol{q}i}A_{\boldsymbol{q}i}^{(n)}}{\omega-\omega_{\boldsymbol{q}i}}, \tag{13}$$

where

$$\omega_{\boldsymbol{q}1,2} = h \pm \omega_{\boldsymbol{q}}^{+-}, \tag{14}$$

$$A_{\boldsymbol{q}1,2}^{(n)} = \frac{1}{2}M^{(n)+-} \pm \frac{1}{2\omega_{\boldsymbol{q}}^{+-}}(\tilde{M}_{\boldsymbol{q}}^{(n)+-} - hM^{(n)+-}), \tag{15}$$

with the moments given by Eqs. (4) and (5). The transverse dynamic spin susceptibility $\chi_{\boldsymbol{q}}^{+-}(\omega)=-\langle\langle S_{\boldsymbol{q}}^+;S_{-\boldsymbol{q}}^-\rangle\rangle_\omega$ is given by Eq. (12) for $n=0$.

Because we consider nonzero magnetic fields within the second-order theory, the behavior of the Green functions (12) with the poles (14) exhibits, for arbitrary spin, a peculiar aspect. Considering the static Green functions $\langle\langle S_{\boldsymbol{q}}^+;S_{-\boldsymbol{q}}^{(n)-}\rangle\rangle_{\omega=0}$, in particular, the static spin susceptibility $\chi_{\boldsymbol{q}}^{+-}\equiv\chi_{\boldsymbol{q}}^{+-}(\omega=0)$, a divergency signaling a phase transition could appear if $\omega_{\boldsymbol{q}2}=0$, i.e., $\omega_{\boldsymbol{q}}^{+-}=h$. According to Eq. (10), the corresponding $\boldsymbol{q}$ values are given by

$$1-\gamma_{\boldsymbol{q}}=g_0\equiv(4z\alpha_1^{+-}C_{10})^{-1}\{[(\Delta^{+-})^2+16\alpha_1^{+-}C_{10}h^2]^{1/2}-\Delta^{+-}\}. \tag{16}$$

This equation may be fulfilled in region I of the h-T plane that is defined by $h<h_0(T)$, where $h_0(T)$ is determined by Eq. (16) with $g_0=2$, which is realized at the corner of the Brillouin zone with $\gamma_{\boldsymbol{q}}=-1$. In region II, $h>h_0(T)$, we have $h>\omega_{\boldsymbol{q}}^{+-}$ for all $\boldsymbol{q}$. For nonzero fields, the Heisenberg ferromagnet that is described by Eq. (1) has no phase transition. This means, $\chi_{\boldsymbol{q}}^{+-}$ has to be finite at all $\boldsymbol{q}$. We require this regularity to hold also for the static Green functions with $n=1,\ldots,2S-1$. That is, in region I, we require $A_{\boldsymbol{q}2}^{(n)}=0$, with $\boldsymbol{q}$ given by Eq. (16). This results in the regularity conditions,

$$hM^{(n)+-}=z\Bigg\{2C_{10}^{(n)zz}+C_{10}^{(n)-+}+(1-\delta_{n,0})\times\sum_{k=1}^{n}\binom{n}{k}(-1)^k[S(S+1)(\delta_{k,n}\langle S^z\rangle+(1-\delta_{k,n})C_{10}^{(n-k-1)zz})+C_{10}^{(n-k)zz}-C_{10}^{(n-k+1)zz}]\Bigg\}g_0. \tag{17}$$

Note that Eq. (17) for $S=1/2$ agrees with the condition given in Ref. 18, which is obtained from an analyticity argument and is written as an expression for $\langle S^z\rangle$. In the limit $T\to\infty$, the field h_0 separating regions I and II may be easily obtained. For $T\to\infty$, we have spin rotational symmetry so that $\langle(S^z)^2\rangle=\frac{1}{2}C_{00}^{(0)-+}$. By Eq. (6) with $\lim_{T\to\infty}\langle S^z\rangle=0$, we get $\langle(S^z)^2\rangle=\frac{1}{3}S(S+1)$, resulting in $\Delta^{+-}=\frac{4}{3}S(S+1)$ and $(\omega_{\boldsymbol{q}}^{+-})^2=\frac{z}{2}\Delta^{+-}(1-\gamma_{\boldsymbol{q}})$. From $\omega_{\boldsymbol{q}}^{+-}=h$ and $g_0=2$, we get $\lim_{T\to\infty}h_0(T)=2\sqrt{zS(S+1)/3}$. Following Ref. 18, we assume conditions (17) to be valid also in region II. This guarantees the continuity of all quantities at the boundary $h_0(T)$.

From the Green functions (12) and (13), the transverse correlators $C_{\boldsymbol{R}}^{(n)-+}=(1/N)\Sigma_{\boldsymbol{q}}C_{\boldsymbol{q}}^{(n)-+}e^{i\boldsymbol{qR}}$ and $\tilde{C}_{\boldsymbol{R}}^{(n)-+}=(1/N)\Sigma_{\boldsymbol{q}}\tilde{C}_{\boldsymbol{q}}^{(n)-+}e^{i\boldsymbol{qR}}$, with the structure factors $C_{\boldsymbol{q}}^{(n)-+}=\langle S_{-\boldsymbol{q}}^{(n)-}S_{\boldsymbol{q}}^{+}\rangle$ and $\tilde{C}_{\boldsymbol{q}}^{(n)-+}=\langle S_{-\boldsymbol{q}}^{(n)-}i\dot{S}_{\boldsymbol{q}}^{+}\rangle$ are calculated by the spectral theorem,

$$C_{\boldsymbol{q}}^{(n)-+}=\sum_{i=1,2}A_{\boldsymbol{q}i}^{(n)}n(\omega_{\boldsymbol{q}i}),\quad \tilde{C}_{\boldsymbol{q}}^{(n)-+}=\sum_{i=1,2}\omega_{\boldsymbol{q}i}A_{\boldsymbol{q}i}^{(n)}n(\omega_{\boldsymbol{q}i}), \tag{18}$$

where $n(\omega)=(e^{\beta\omega}-1)^{-1}$ and $\beta=1/T$.

Now, we derive some useful sum rules. By using $\langle S_i^{(n)-}S_i^{+}\rangle=\langle(S_i^z)^nS_i^-S_i^+\rangle$ that is obtained from Eq. (6) multiplied by $(S_i^z)^n$ $(n=0,1,\ldots,2S-1)$ and Eq. (18), we get the relation

$$S(S+1)\langle(S^z)^n\rangle-\langle(S^z)^{n+1}\rangle-\langle(S^z)^{n+2}\rangle=\frac{1}{N}\sum_{\boldsymbol{q}}\sum_{i=1,2}A_{\boldsymbol{q}i}^{(n)}n(\omega_{\boldsymbol{q}i}). \tag{19}$$

By the identity $\Pi_{m=-S}^{S}(S_i^z-m)=0$, one can express $(S_i^z)^{2S+1}$ appearing in Eq. (19) for $n=2S-1$ in terms of lower powers of S_i^z (Refs. 16 and 25),

$$(S_i^z)^{2S+1}=\sum_{k=0}^{2S}\alpha_k^{(S)}(S_i^z)^k, \tag{20}$$

where the coefficients $\alpha_k^{(S)}$ are given in Ref. 25. From the system of the $2S$ equations (19), we can determine the magnetization $m=-2\mu_B\langle S^z\rangle$.

Similarly, in the second-order theory, higher-derivative sum rules may be derived, which, for nonzero fields, provide $2S$ additional equations for determining the vertex parameters and some longitudinal correlators (see below). By multiplying $S_i^{(n)-}$ by $i\dot{S}_i^{+}=\Sigma_{j(n.n.i)}(S_j^zS_i^+-S_j^+S_i^z)+hS_i^+$ and by using Eqs. (13), (14), (18), and (6), we obtain

$$z\{S(S+1)[\delta_{n,0}\langle S^z\rangle+(1-\delta_{n,0})C_{10}^{(n-1)zz}]-C_{10}^{(n)zz}-C_{10}^{(n+1)zz}-C_{10}^{(n)-+}-C_{10}^{(n+1)-+}\}=-\frac{1}{N}\sum_{\boldsymbol{q}}\sum_{i=1,2}(-1)^i\omega_{\boldsymbol{q}i}^{+-}A_{\boldsymbol{q}i}^{(n)}n(\omega_{\boldsymbol{q}i}). \tag{21}$$

The correlator $C_{10}^{(n+1)zz}$ for $n=2S-1$ may be expressed in terms of $\langle S^z\rangle$ and $C_{10}^{(n)zz}$ with $n\leqslant 2S-1$ by Eq. (20). Equally, $C_{10}^{(2S)-+}$ can be written in terms of $C_{10}^{(n)-+}$ $(n\leqslant 2S-1)$ by the identity[25]

$$S_i^-(S_i^z)^{2S}=S_i^-\sum_{k=0}^{2S-1}\delta_k^{(S,1)}(S_i^z)^k, \tag{22}$$

where the coefficients $\delta_k^{(S,1)}$ are given in Ref. 25. The product $(S_i^z)^{2S}S_i^-$ appearing in $C_{10}^{(2S)-+}$ can be deduced from Eq. (22) by the commutation relations for spin operators. The sum rule (21) for $n=0$ also follows from the exact representation of the internal energy per site, $u=\langle H\rangle/N=-\frac{z}{2}(C_{10}^{(0)-+}+C_{10}^{(0)zz})-h\langle S^z\rangle$, in terms of $\langle\langle S_{\boldsymbol{q}}^+;S_{-\boldsymbol{q}}^-\rangle\rangle_\omega$, which can be similarly derived as in Ref. 26 for $S=1/2$,

$$u=-\frac{z}{2}[S(S+1)\langle S^z\rangle-C_{10}^{(1)zz}-C_{10}^{(1)-+}]-h\langle S^z\rangle-\frac{1}{N}\sum_{\boldsymbol{q}}\int_{-\infty}^{+\infty}\frac{d\omega}{2\pi}(\omega-h)\mathrm{Im}\langle\langle S_{\boldsymbol{q}}^+;S_{-\boldsymbol{q}}^-\rangle\rangle_\omega n(\omega), \tag{23}$$

if the result [Eq. (12)] for $\langle\langle S_{\boldsymbol{q}}^+;S_{-\boldsymbol{q}}^-\rangle\rangle_\omega$ $(n=0)$ is inserted into Eq. (23).

To calculate the longitudinal spin correlation functions $C_{\boldsymbol{R}}^{(0)zz}$ from the Green function $\langle\langle S_{\boldsymbol{q}}^z;S_{-\boldsymbol{q}}^z\rangle\rangle_\omega=-\chi_{\boldsymbol{q}}^{zz}(\omega)$, where $\chi_{\boldsymbol{q}}^{zz}(\omega)$ is the longitudinal dynamic spin susceptibility, we start from the equations of motion analogous to Eqs. (2) and (3) and perform a second-order decoupling, which is equivalent to the projection method with the basis $(S_{\boldsymbol{q}}^z,i\dot{S}_{\boldsymbol{q}}^z)$ neglecting the self-energy, as indicated in our previous papers.[17,20] In $-\ddot{S}_i^z$, we adopt the decouplings[17,19,20] analogous to Eqs. (7) and (8),

$$S_i^zS_j^+S_l^-=\alpha_1^{zz}\langle S_j^+S_l^-\rangle S_i^z, \tag{24}$$

$$S_i^+S_j^zS_l^-=\alpha_2^{zz}\langle S_i^+S_l^-\rangle S_j^z, \tag{25}$$

where $\langle i,j,l\rangle$ form NN sequences, and

$$S_i^- S_j^z S_j^+ = \lambda^{zz} \langle S_i^- S_j^+ \rangle S_j^z. \tag{26}$$

We obtain

$$\chi_q^{zz}(\omega) = -\frac{M_q^{zz}}{\omega^2 - (\omega_q^{zz})^2}, \tag{27}$$

with $M_q^{zz} = \langle [i\dot{S}_q^z, S_{-q}^z] \rangle$ given by

$$M_q^{zz} = zC_{10}^{(0)-+}(1-\gamma_q), \tag{28}$$

and

$$(\omega_q^{zz})^2 = \frac{z}{2}(1-\gamma_q)\{\Delta^{zz} + 2z\alpha_1^{zz} C_{10}^{(0)-+}(1-\gamma_q)\}, \tag{29}$$

$$\Delta^{zz} = 2\{S(S+1) - \langle (S^z)^2 \rangle + [\lambda^{zz} - (z+1)\alpha_1^{zz}] C_{10}^{(0)-+} + \alpha_2^{zz}[(z-2)C_{11}^{(0)-+} + C_{20}^{(0)-+}]\}. \tag{30}$$

As for the transverse correlations [cf. Eq. (11)], in the case $S=1/2$, we have $\lambda^{zz}=0$. The correlation functions $C_{\boldsymbol{R}}^{(0)zz}$ are calculated from[17]

$$C_{\boldsymbol{R}}^{(0)zz} = \frac{1}{N}\sum_{\boldsymbol{q}(\neq 0)} C_{\boldsymbol{q}}^{zz} e^{i\boldsymbol{q}\boldsymbol{R}} + \langle S^z \rangle^2, \tag{31}$$

with

$$C_q^{zz} = \frac{M_q^{zz}}{2\omega_q^{zz}}[1 + 2n(\omega_q^{zz})]. \tag{32}$$

Let us consider the magnetic susceptibility $\chi = 4\mu_B^2 \chi_S$ with $\chi_S = \partial \langle S^z \rangle / \partial h$, which we denote by isothermal susceptibility, and its relation to the Kubo susceptibility [Eq. (27)]. From the first and the second derivatives of the partition function with respect to h, we obtain the exact relation

$$\chi_S = \frac{1}{T}\sum_{\boldsymbol{R}} \bar{C}_{\boldsymbol{R}}^{(0)zz} = \frac{1}{T}\bar{C}_{q=0}^{zz}, \tag{33}$$

where $\bar{C}_{\boldsymbol{R}}^{(0)zz} = C_{\boldsymbol{R}}^{(0)zz} - \langle S^z \rangle^2$, and the Fourier transform reads $\bar{C}_q^{zz} = C_q^{zz} - N\langle S^z \rangle^2 \delta_{q,0}$. By Eqs. (27) and (32), the uniform static Kubo susceptibility $\chi_0^{zz} = \lim_{q\to 0} \lim_{\omega \to 0} \chi_q^{zz}(\omega)$ may be expressed as $\chi_0^{zz} = \frac{1}{T} \lim_{q\to 0} C_q^{zz} = \frac{1}{T} \lim_{q\to 0} \bar{C}_q^{zz} = \frac{1}{T}\bar{C}_{q=0}^{zz}$. That is, within our theory, the isothermal and Kubo susceptibilities agree at arbitrary fields and temperatures. By using Eqs. (27)–(29), we have

$$\frac{\partial \langle S^z \rangle}{\partial h} = \frac{2C_{10}^{(0)-+}}{\Delta^{zz}}. \tag{34}$$

Equality (34) is an additional equation for determining the parameters of the theory. By considering the ground state ($T=0$), we have the exact results

$$C_{\boldsymbol{R}}^{(n)-+}(0) = 0, \quad C_{\boldsymbol{R}}^{(n)zz}(0) = S^{2+n}, \quad \langle (S^z)^n \rangle (0) = S^n. \tag{35}$$

The regularity conditions [Eq. (17)] read as $g_0 = h/zS$. From $g_0=2$, the field $h_0(0)$ is given by $h_0(0) = 2zS$. By taking g_0 from Eq. (16), we get the equation $\Delta^{+-} = 2(1-\alpha_1^{+-})hS$. This equation can be fulfilled only if $\alpha_1^{+-}(0)=1$ and $\Delta^{+-}(0)=0$ because in the ground state of the ferromagnet at $h \neq 0$, all quantities do not depend on h. By taking Δ^{+-} from Eq. (11), we get the parameter relation $\lambda^{+-}(0) + (z-1)\alpha_2^{+-}(0) = z - 1/2S$. For $S=1/2$ ($\lambda^{+-}=0$), we have $\alpha_2^{+-}(0)=1$. Concerning the zero-temperature values of α_1^{zz} and Δ^{zz}, they can be determined only in the limit $T \to 0$ since Eqs. (31) and (32) for $C_{\boldsymbol{R}}^{(0)zz}$ contain M_q^{zz} with $\lim_{T\to 0} M_q^{zz} = 0$.

To evaluate the thermodynamic properties for arbitrary spin, the transverse correlators $C_{10}^{(n)-+}$, the longitudinal correlators ($\langle (S^z)^{n+1} \rangle$, $C_{10}^{(n)zz}$), and the parameters $\alpha_1^{\nu\mu}$ and $\Delta^{\nu\mu}$ ($\mu\nu = -+, zz$) have to be determined as solutions of a coupled system of self-consistency equations for arbitrary temperatures and fields. Note that for $S > 1/2$, the parameters $\alpha_2^{\nu\mu}$ and $\lambda^{\nu\mu}$ have not to be separately calculated because they only appear in the combination given by $\Delta^{\nu\mu}$. The correlation functions $C_{10}^{(n)-+}$ are calculated from the Green functions according to Eqs. (18). To determine the $4(S+1)$ quantities $\langle (S^z)^{n+1} \rangle$ and $C_{10}^{(n)zz}$ with $n = 0, \ldots, 2S-1$, $\alpha_1^{\nu\mu}$, and $\Delta^{\nu\mu}$, we have $6S+3$ equations, namely, the regularity conditions [Eq. (17)], the sum rules [Eqs. (19) and (21)], Eqs. (31) for $\langle (S^z)^2 \rangle$ and $C_{10}^{(0)zz}$, and equality (34). That is, for $S > 1/2$, we have $2S-1$ more equations than quantities to be determined. To obtain a closed system of self-consistency equations for $S > 1/2$, i.e., to reduce the number of equations (in addition to those for $C_{10}^{(n)-+}$) to $4(S+1)$, we consider two choices. First, we take into account the higher-derivative sum rule [Eq. (21)] with $n=0$ only. As revealed by numerical evaluations, the specific heat of the 1D model strongly deviates from the QMC data for $S=1$, and for $S>1$, it even becomes negative at low fields and temperatures. Therefore, we adopt another choice, which yields a good agreement of all thermodynamic quantities with the QMC data for $S=1$ and which is used for $S \geqslant 1$ throughout the paper. Namely, we take into account the higher sum rules [Eq. (21)] with $n=0$ and with $n=1$ instead of Eq. (31) for $C_{10}^{(0)zz}$. To justify this choice within the theory itself, the correlator $C_{10}^{(0)zz}$ resulting from the closed system of equations is compared to $C_{10}^{(0)zz}$ that is calculated by Eq. (31). For example, in the 1D $S=1$ model at the fields $h=0.05$ and 0.1, the deviation is found to be less than 2% at all temperatures except for the region $0.1 \lesssim T \lesssim 1$, where the maximal deviation is about 9% for $T \simeq 0.3$ and 0.4, respectively. From the solution of the self-consistency equations in region I and from Eq. (16) with $g_0=2$, the boundary between regions I and II, $h_0(T)$, is determined. In Fig. 1, $h_0(T)$ is plotted for $S=1/2$ and $S=1$. Note that in experiments realistic values of temperature and field lie in region I. Therefore, below nearly all results are presented in this region, and only some results for high enough temperatures and fields in region II are shown in Fig. 7.

Let us finally make some comments on the evaluation of the theory for different spin values.

(i) $S=\frac{1}{2}$: By using the identities $(S_i^z)^2 = 1/4$ and $S_i^z S_i^- = -\frac{1}{2}S_i^-$ [cf. Eq. (22)], the sum rules [Eqs. (19) and (21)] for $n=0$ simplify, where the higher sum rule [Eq. (21)] reduces to

$$z\left(\frac{1}{2}\langle S^z \rangle - C_{10}\right) = -\frac{1}{N}\sum_{\boldsymbol{q},i} (-1)^i \omega_{\boldsymbol{q}i}^{+-} A_{\boldsymbol{q}i}^{(0)} n(\omega_{\boldsymbol{q}i}). \tag{36}$$

Note that this sum rule may also be obtained from the exact representation [Eq. (23)] of the internal energy, which in the case $S=1/2$ becomes (cf. Ref. 17)

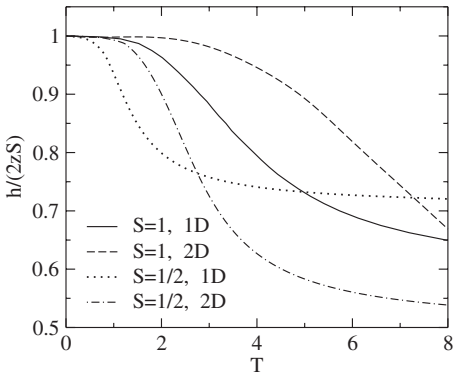

FIG. 1. Boundary $h_0(T)$ in the $h-T$ plane separating region I, $h<h_0(T)$, where the equality $\omega_{\boldsymbol{q}}^{+-}=h$ [cf. Eq. (14)] may be fulfilled, from region II, $h>h_0(T)$, where $h>\omega_{\boldsymbol{q}}^{+-}$ for all $\boldsymbol{q}$.

$$u=-\frac{z}{8}-\frac{h}{2}-\frac{1}{N}\sum_{\boldsymbol{q}}\int_{-\infty}^{+\infty}\frac{d\omega}{2\pi}(\varepsilon_{\boldsymbol{q}}+\omega)\mathrm{Im}\langle\langle S_{\boldsymbol{q}}^{+};S_{-\boldsymbol{q}}^{-}\rangle\rangle_{\omega}n(\omega), \tag{37}$$

with $\varepsilon_{\boldsymbol{q}}=z(1-\gamma_{\boldsymbol{q}})/2+h$ if $\langle\langle S_{\boldsymbol{q}}^{+};S_{-\boldsymbol{q}}^{-}\rangle\rangle_{\omega}$ that is given by Eq. (12) for $n=0$ is inserted into Eq. (37). The spectra $\omega_{\boldsymbol{q}}^{+-}$ and $\omega_{\boldsymbol{q}}^{zz}$ are given by Eqs. (10), (11), (29), and (30) with $\lambda^{+-}=0$ and $\lambda^{zz}=0$. We have to solve a closed system of coupled self-consistency equations for the seven quantities $\langle S^z\rangle$, $C_{10}^{(0)\mu\nu}$, $\alpha_1^{\nu\mu}$, and $\Delta^{\nu\mu}$ (or $\alpha_2^{\nu\mu}$). Note that in previous approaches,[17,18] the simplified choice $\alpha_2^{\nu\mu}=\alpha_1^{\nu\mu}$ is taken disregarding equality (34) and not by using either condition (17) (Ref. 17) or the higher sum rule [Eq. (36)] (Ref. 18).

(ii) $S\geqslant 1$: Let us specify identities (20) and (22), which are used to reduce the sum rules [Eqs. (19) and (21)] for $n=2S-1$, respectively, for $S=1$ and $S=3/2$. For $S=1$, we have $(S_i^z)^3=S_i^z$ and $(S_i^z)^2S_i^-=-S_i^zS_i^-$, and for $S=3/2$, we get $(S_i^z)^4=\frac{5}{2}(S_i^z)^2-\frac{9}{16}$ and $(S_i^z)^3S_i^-=-\frac{3}{2}(S_i^z)^2S_i^-+\frac{1}{4}S_i^zS_i^-+\frac{3}{8}S_i^-$. For $S=1$, a closed system of coupled self-consistency equations for the ten quantities $\langle S^z\rangle$, $\langle(S^z)^2\rangle$, $C_{10}^{(0)\mu\nu}$, $C_{10}^{(1)\mu\nu}$, $\alpha_1^{\nu\mu}$, and $\Delta^{\nu\mu}$ has to be solved.

In the case $h=0$, we have $\langle S^z\rangle=0$, and the correlators for $n=0$ only are needed. The spin-rotation symmetry, implying $C_{\boldsymbol{R}}^{(0)-+}=2C_{\boldsymbol{R}}^{(0)zz}=C_{\boldsymbol{R}}$, is preserved by the second-order theory with $\alpha_{1,2}^{+-}=\alpha_{1,2}^{zz}\equiv\alpha_{1,2}$ and $\lambda^{+-}=\lambda^{zz}\equiv\lambda$. By using $\langle(S^z)^2\rangle=\frac{1}{3}S(S+1)$ following from Eq. (6), Eqs. (10), (11), (29), and (30) yield the spectrum $\omega_{\boldsymbol{q}}^{+-}=\omega_{\boldsymbol{q}}^{zz}\equiv\omega_{\boldsymbol{q}}$ given by

$$\omega_{\boldsymbol{q}}^2=\frac{z}{2}(1-\gamma_{\boldsymbol{q}})\{\Delta+2z\alpha_1C_{10}(1-\gamma_{\boldsymbol{q}})\}, \tag{38}$$

with

$$\Delta=\frac{4}{3}S(S+1)+2\{\lambda-(z+1)\alpha_1\}C_{10}+2\alpha_2\{(z-2)C_{11}+C_{20}\}, \tag{39}$$

which agrees with the result of Ref. 19 if we set $\alpha_2=\alpha_1$.

The susceptibility $\chi_S=\chi_0^{zz}$ resulting from Eq. (34) is given by $\chi_S=2C_{10}/\Delta$. The correlators $C_{\boldsymbol{R}}^{(0)zz}$ are calculated from Eqs. (31) and (32) with $\langle S^z\rangle^2$ replaced by $C^{zz}\equiv(1/N)\Sigma_{\boldsymbol{R}}C_{\boldsymbol{R}}^{(0)zz}$ (see Refs. 21 and 23), where the condensation part C^{zz} describes long-range order (LRO). At $T=0$, we have the exact result $C_{\boldsymbol{R}\neq 0}^{(0)zz}=\frac{1}{3}S^2$. The ferromagnetic LRO is reflected in the divergence of χ_S so that $\Delta(0)=\frac{4}{3}S(S+1)+\frac{4}{3}S^2\{\lambda-(z+1)\alpha_1+(z-1)\alpha_2\}=0$ and $\omega_{\boldsymbol{q}}=z\sqrt{2\alpha_1/3}S(1-\gamma_{\boldsymbol{q}})$. Then, by using Eq. (31), we get $C_{\boldsymbol{R}}^{(0)zz}(0)=S/\sqrt{6\alpha_1}\delta_{\boldsymbol{R},0}+C^{zz}$, resulting in the sum rule [$\boldsymbol{R}=0$, cf. Eq. (6)] $\frac{1}{3}S(S+1)=S/\sqrt{6\alpha_1}+C^{zz}$, and in $C^{zz}=\frac{1}{3}S^2(\boldsymbol{R}\neq 0)$. Finally, at $T=0$, we obtain $\alpha_1(0)=3/2$ and $\lambda(0)+(z-1)\alpha_2(0)=\frac{1}{2}(3z+1)-1/S$. For $S=1/2$ ($\lambda=0$), we have $\alpha_2(0)=\alpha_1(0)=3/2$. At finite temperatures, there is no LRO in the 1D and 2D systems implying $C^{zz}=0$. The higher sum rule [Eq. (21)] for $n=0$ or, equivalently, Eq. (23) turns out to be trivially fulfilled. Therefore, following Ref. 19, we set $\alpha_2=\alpha_1\equiv\alpha$ and $\lambda(T)=\lambda(0)=2-1/S$ and determine $\alpha(T)$ from the sum rule $C_0^{(0)zz}=\frac{1}{3}S(S+1)$.

III. QUANTUM MONTE CARLO SIMULATIONS

In order to assess the accuracy of the approximations that are employed in the Green-function theory that is presented in the previous section, we perform QMC simulations. The Heisenberg ferromagnets with $S=1/2$ and $S=1$ that are placed on chains or square lattices with periodic boundary conditions are simulated by using the stochastic series expansion method,[27,28] which utilizes the high-temperature series expansion,

$$Z=\mathrm{Tr}\,e^{-\beta H}=\sum_{\alpha}\sum_{n=0}^{\infty}\frac{\beta^n}{n!}\langle\alpha|(-H)^n|\alpha\rangle, \tag{40}$$

where the first sum is over a complete set of states $|\alpha\rangle$, which is usually taken as the eigenvectors of the S_i^z operator. By decomposing the Hamiltonian into diagonal and off-diagonal bond operators, introducing constant unit operators to assure positivity, and re-expanding Eq. (40), one finally ends up with a nonlocal loop representation, which allows very efficient sampling.[27,28] To minimize the effect of self-crossing and backtracking, the directed loop-updating scheme is employed.

After initial thermalization with about 10^6 Monte Carlo steps, the measurements are made after each step. During the simulation, the energy, magnetization, and correlation functions are measured and stored in a time series file, from which the specific heat and magnetic susceptibility can be computed by using the fluctuation-dissipation relation. The correlation lengths are extracted from the exponential falloff of the correlation functions and for comparison also by means of the second-moment method.[29] Only for correlations smaller than one lattice spacing, small systematic deviations are visible. All those observables can be easily expressed by states of the spins on the lattice and the number and types of operators.[30] The whole simulation usually takes of the order of 10^7 Monte Carlo steps. The statistical error bars are estimated by the Jackknife method.[31]

The results that are presented in this paper are generated for $S=1/2$ chains of length up to $L=1024$ and for $S=1$ up to $L=64$. In two dimensions, we simulate square lattices of edge length up to $L=64$. By comparing the results for different lattice sizes, we made sure that for the investigated range

of temperatures and fields, the thermodynamic limit of the considered observables lies within the statistical error bars of the numerical results.

IV. RESULTS

As described in Sec. II, the quantities of the Green-function theory determining the thermodynamic properties have to be numerically calculated as solutions of a coupled system of nonlinear algebraic self-consistency equations. To this end, we use Broyden's method,[32] which yields the solutions with a relative error of about 10^{-7} on the average, where the numerical error increases with decreasing field and temperature. The momentum integrals occurring in the self-consistency equations are done by using Gaussian integration. Considering the $S=1/2$ ferromagnet in Refs. 17 and 18, the thermodynamic quantities, except for the transverse and longitudinal correlation lengths, are calculated. Therefore, we present only some results for $S=1/2$ (see Figs. 3, 7, and 15), which visibly improve those of Ref. 17.

A. Magnetic susceptibility

Let us first consider the susceptibility χ_S in the case $h=0$, $\chi_S=2C_{10}/\Delta$ (see Sec. II). In one dimension, the low-temperature expansion yields $\lim_{T\to 0}\chi_S T^2=\frac{2}{3}S^4$ (Ref. 19). Note that this result agrees with that obtained by the modified spin-wave theory (MSWT).[33] For $S=1/2$, we have $\lim_{T\to 0}\chi_S T^2=0.041\,667$, which is in very good agreement with the Bethe-ansatz value $\lim_{T\to 0}\chi_S T^2=0.041\,675$ (Ref. 34). On the other hand, previous QMC simulations by Handscomb's method on an $N=256$ chain combined with a renormalization-group approach[35] yield $\lim_{T\to 0}\chi_S T^2=0.0329$ (note that χ plotted in Ref. 35 and defined in Ref. 36 is related to χ_S by $\chi=3\chi_S/S^2$). To resolve the discrepancy between the QMC results of Ref. 35 and the Bethe-ansatz value, we perform QMC simulations for chains up to $N=1024$ sites. The results at very low temperatures are shown in Fig. 2 (taking the same plot as in Ref. 35) and compared to the Bethe-ansatz data,[34] the QMC data of Ref. 35, and to the Green-function theory. Above a characteristic temperature, which decreases with increasing chain length, our QMC data agree very well with the Bethe-ansatz results. On the contrary, the QMC results of Ref. 35 for $\chi_S T^2$ are lower than ours by 4% on the average. To determine the limit $\lim_{T\to 0}\chi_S T^2$ from our QMC data, we perform a finite-size scaling analysis. To this end, for each chain length, we linearly extrapolate the low-temperature linear part of the curve $\chi_S T^2$ to $T=0$ and fit the limiting values as function of $1/N$ by a linear dependence (see inset of Fig. 2). The extrapolation to $1/N=0$ yields $\lim_{N\to\infty}\lim_{T\to 0}\chi_S T^2=0.0413\pm 0.0005$, which agrees, within the given statistical error, with the Bethe-ansatz value.

The 2D zero-field susceptibility in the second-order Green-function theory exponentially increases for $T\to 0$, $\chi_S \propto \exp(2\pi S^2/T)$ (Ref. 19), where the exponent is smaller by a factor of 2 compared to that found in the MSWT[33] and in the renormalization-group approach.[36]

Now, we consider nonzero fields and calculate the susceptibility $\chi_S=\partial\langle S^z\rangle/\partial h$. First, we show the magnetization. For

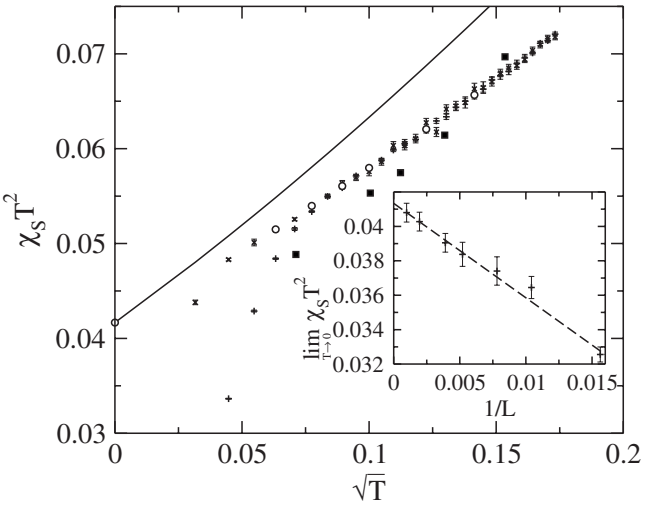

FIG. 2. Zero-field susceptibility of the 1D $S=1/2$ ferromagnet. The results of the Green-function theory (solid line) and the QMC data (+: $L=256$ and ×: $L=1024$) are compared to the QMC data of Ref. 35 (■) and the Bethe-ansatz results of Ref. 34 (○). In the inset, the finite-size scaling of the zero-temperature limit of $\chi_S T^2$ that is calculated by QMC is depicted. The dashed line shows the least-squares fit of the data by a linear dependence.

$S=1/2$, as an example, $\langle S^z\rangle$ in the 1D model is depicted in the inset of Fig. 3. For the $S=1$ ferromagnet, our analytical and QMC results in comparison to the RPA are plotted in Fig. 4. Let us emphasize the excellent agreement of the theory for the chain [Fig. 4(a)] with the QMC data over the whole temperature and field regions. For the 1D ferromagnet, the RPA is a remarkably good approximation for $\langle S^z\rangle$, as was also found in the case $S=1/2$.[17] In two dimensions [Fig. 4(b)], as compared to the QMC data, the results of our theory at higher temperatures are somewhat worse than those of the

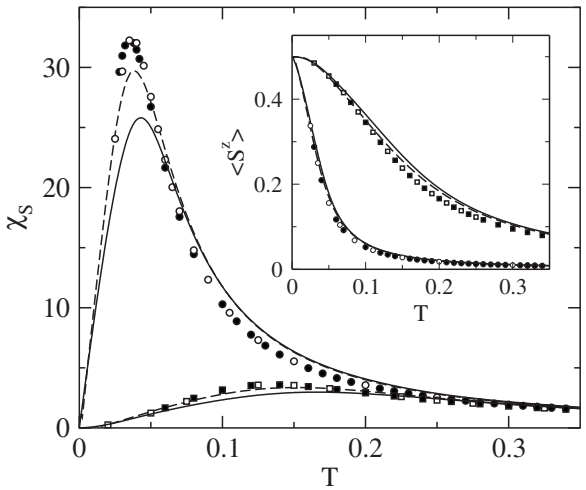

FIG. 3. Susceptibility of the 1D $S=1/2$ ferromagnet at $h=0.005$ and 0.05, from top to bottom, where the results of the Green-function theory (solid lines) and of the Green-function method of Ref. 18 (dashed lines), the QMC data (filled symbols, $L=128$), and the Bethe-ansatz results of Ref. 17 (open symbols) are shown. In the inset, the 1D magnetization at $h=0.005$ and 0.05, from bottom to top, is depicted.

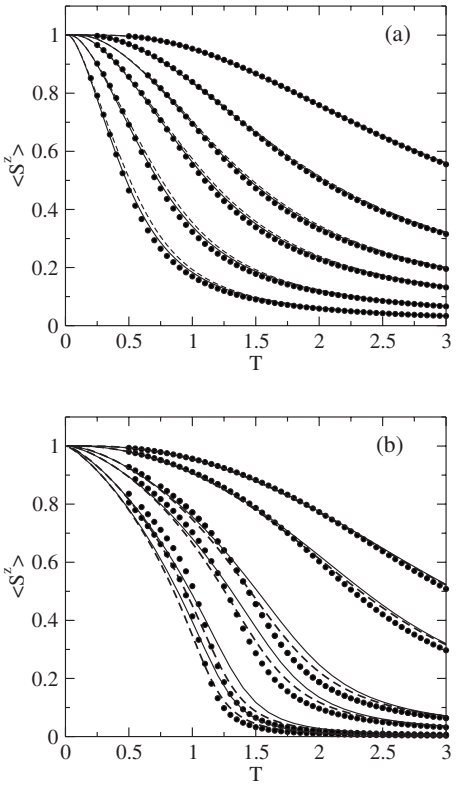

FIG. 4. Magnetization of the (a) 1D and (b) 2D $S=1$ ferromagnet in magnetic fields of strengths (a) $h=0.1$, 0.2, 0.4, 0.6, 1.0, and 2.0, from bottom to top, and (b) $h=0.005$, 0.01, 0.05, 0.1, 0.5, and 1.0, from bottom to top, as obtained by the Green-function theory (solid lines) and by the QMC method for $L=64$ (●) compared to RPA results (dashed lines).

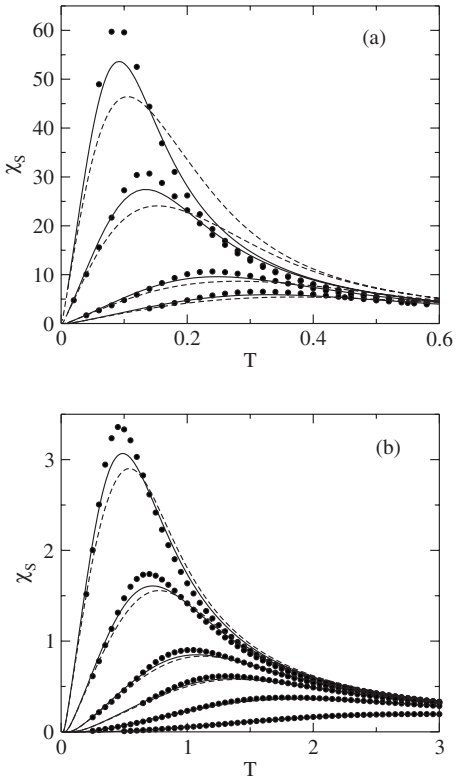

FIG. 5. Susceptibility of the 1D $S=1$ ferromagnet (a) at low fields, $h=0.005$, 0.01, 0.03, and 0.05, from top to bottom, and (b) at higher fields, $h=0.1$, 0.2, 0.4, 0.6, 1.0, and 2.0, from top to bottom, where the Green-function (solid lines), the QMC (●, $L=64$), and the RPA results (dashed lines) are shown.

RPA. This is in contrast to the 2D $S=1/2$ ferromagnet, for which we obtain slightly better results than the RPA at all temperatures and fields (improving our previous findings[17]).

The susceptibility for $h\neq 0$ vanishes at $T=0$. Therefore, $\chi_S(T)$ has a maximum at T_m^χ, where T_m^χ increases and the height of the susceptibility maximum $\chi_S(T_m^\chi)$ decreases with increasing field. For $S=1/2$, in Fig. 3, the low-field susceptibility in the 1D model is shown, where for $h=0.005$ a better agreement of the theory with the Bethe-ansatz results is found than in Ref. 17. Note that our QMC data are in a very good agreement with the Bethe results. For comparison, in Fig. 3, the susceptibility in the simplified approach with $\alpha_2^{\nu\mu}=\alpha_1^{\nu\mu}$ (Ref. 18), where equality (34) is disregarded and the regularity condition (17) is used instead of the higher sum rule [Eq. (36)], is plotted as well. It is remarkable that χ_S in this approach is in a better agreement with the exact methods than the susceptibility in our extended theory with $\alpha_2^{\nu\mu}\neq\alpha_1^{\nu\mu}$. However, considering the correlation length the situation changes qualitatively (see below). For $S=1$, the susceptibility is plotted in Figs. 5 and 6. In one dimension (Fig. 5), good agreement between Green-function theory and QMC corresponds to the results depicted in Fig. 4(a). As compared to the QMC data for the 2D model (Fig. 6) in RPA, the maximum position T_m^χ is somewhat better reproduced than in our theory.

To analyze the field dependence of T_m^χ and $\chi_S(T_m^\chi)$ in more detail as in our previous paper,[17] the calculations are extended to a much broader field region, $0.001\leqslant h\leqslant 10$. As can be seen in Fig. 7(a) at low fields, the theory may be well fitted by the power law,

$$T_m^\chi = ah^\gamma, \tag{41}$$

where the field regions and the values of a and γ are given in Table I. Let us point out that the theory for the 1D $S=1/2$ model is in reasonable agreement with the Bethe-ansatz result at $h\leqslant 0.1$,[17] $a=0.765$, and $\gamma=0.576$. In the high-field region, T_m^χ obeys a linear dependence [cf. inset of Fig. 7(a)],

$$T_m^\chi = \tilde{a}h + \tilde{b}, \tag{42}$$

where $\tilde{a}$ and $\tilde{b}$ are given in Table I. Note that the linear law [Eq. (42)] was not found in Ref. 17. Our results for the maximum height $\chi_S(T_m^\chi)$ as a function of h may be well described in the whole field region $0.001\leqslant h\leqslant 10.0$ [see Fig. 7(b)] by using the power law,

$$\chi_S(T_m^\chi) = bh^\beta, \tag{43}$$

where the coefficients are given in Table II. The values of b and β for $S=1/2$ slightly deviate (by about 5% on the average) from those previously found.[17] Again, our theory for $S=1/2$ is in reasonable agreement with the 1D Bethe-ansatz result at $h\leqslant 0.1$, $b=0.208$, and $\beta=-0.952$ (Ref. 17).

For comparison, we consider the power-law behavior in RPA. We find the RPA results in the low- and high-field

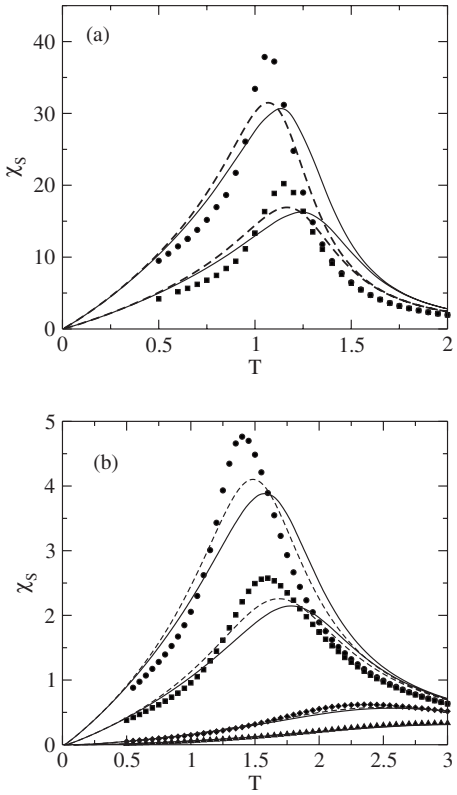

FIG. 6. Susceptibility of the 2D $S=1$ ferromagnet (a) at very low fields, $h=0.005$ and 0.01, from top to bottom, and (b) at higher fields, $h=0.05$, 0.1, 0.5, and 1.0, from top to bottom, which are obtained by the Green-function theory (solid lines), by the QMC for $L=64$ (filled symbols), and by the RPA (dashed lines).

regions to be well fitted by laws (41)–(43), where the coefficients are in good agreement with the values given in Tables I and II. More precisely, for the 1D and 2D $S=1/2$ and $S=1$ models, the average deviations of the coefficients in laws (41)–(43) amount to about 6%, 3%, and 2%, respectively. For example, considering the $S=1/2$ ferromagnet in high fields, $2\leqslant h\leqslant 10$, we obtain the linear dependence [Eq. (42)] for the 1D (2D) case with $\tilde{a}=0.657$ (0.661) and $\tilde{b}=0.496$ (1.015), which yields a better fit than the power law [Eq. (41)]. Recently, in Ref. 37, such a law was given for the 1D (2D) model in region 3 $(4.4)\leqslant h\leqslant 6.5$. Even in this limited field region, we find the fit by the linear law [Eq. (42)] to be slightly better than the fit by the power law [Eq. (41)] (see Ref. 37).

B. Correlation length

To obtain the transverse and longitudinal correlation lengths ξ^{+-} and ξ^{zz}, we consider the long-distance correlators $C_{\boldsymbol{R}}^{(0)-+}$ and $\bar{C}_{\boldsymbol{R}}^{(0)zz}\equiv C_{\boldsymbol{R}}^{(0)zz}-\langle S^z\rangle^2$, with $C_{\boldsymbol{R}}^{(0)zz}$ calculated by Eq. (31), respectively. Note that the temperature dependence of both $C_{\boldsymbol{R}}^{(0)-+}$ and $\bar{C}_{\boldsymbol{R}}^{(0)zz}$ exhibits a maximum because the correlators vanish at $T=0$ [following from Eqs. (31) and (35)] and for $T\to\infty$. By the asymptotic ansatz,

$$C_{\boldsymbol{R}}^{(0)-+}=A^{+-}\exp(-R/\xi^{+-}), \tag{44}$$

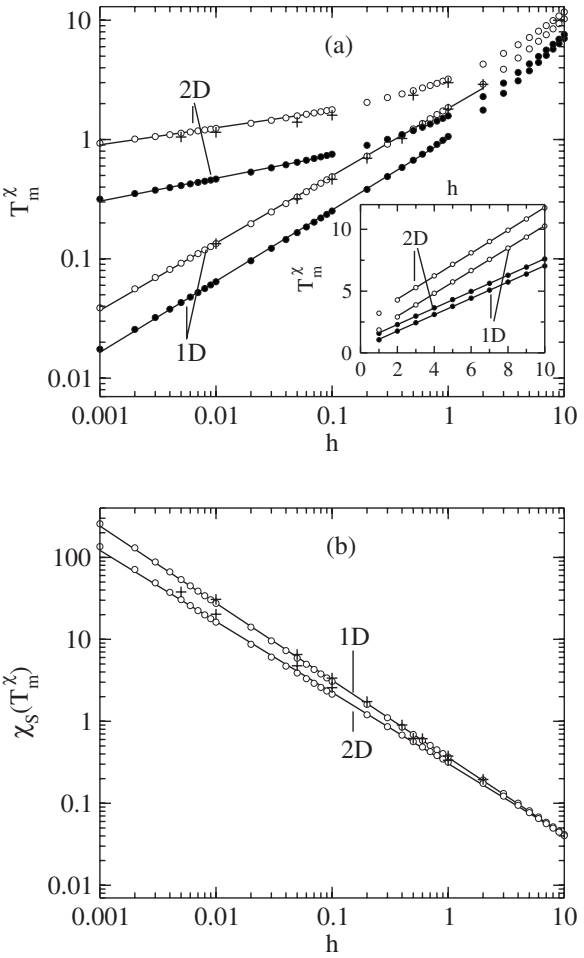

FIG. 7. Field dependence of the (a) position and (b) height of the susceptibility maximum that are obtained by the Green-function theory for the $S=1/2$ (●) and $S=1$ (○) ferromagnets and fit by power laws (solid lines) in comparison to the QMC data (+, $S=1$, $L=64$). The inset shows the fit of T_m^χ at high fields by a linear dependence. For clarity, $\chi_S(T_m^\chi)$ is plotted for $S=1$ only.

$$\bar{C}_{\boldsymbol{R}}^{(0)zz}=A^{zz}\exp(-R/\xi^{zz}), \tag{45}$$

and the logarithmic plot of the correlators as functions of $R=|\boldsymbol{R}|$ the inverse correlation lengths are numerically evaluated from linear fits.

TABLE I. Validity regions (h) and coefficients of the power laws [Eqs. (41) and (42)] for the susceptibility of the 1D and 2D $S=1/2$ and $S=1$ ferromagnets.

	$S=1/2$		$S=1$	
	1D	2D	1D	2D
h	0.001–1.0	0.001–0.1	0.001–2.0	0.001–0.1
a	1.013	1.149	1.823	2.433
γ	0.596	0.192	0.565	0.144
h	1.0–10.0	1.0–10.0	2.0–10.0	2.0–10.0
$\tilde{a}$	0.661	0.666	0.917	0.929
$\tilde{b}$	0.443	0.961	1.136	2.494

TABLE II. Coefficients of the power law [Eq. (43)] for the susceptibility of the 1D and 2D $S=1/2$ and $S=1$ ferromagnets in the field region $0.001 \leqslant h \leqslant 10.0$.

	$S=1/2$		$S=1$	
	1D	2D	1D	2D
b	0.192	0.166	0.362	0.305
β	−0.925	−0.850	−0.941	−0.867

In the literature, often the correlation length is determined from the expansion of the static spin susceptibility around the magnetic wave vector (see, e.g., Refs. 23, 21, and 20). In the ferromagnetic case, we expand the static susceptibilities $\chi_{\boldsymbol{q}}^{+-}$ [resulting from Eqs. (10)–(12), (14), and (15)] and $\chi_{\boldsymbol{q}}^{zz}$ [given by Eqs. (27)–(29)] around $\boldsymbol{q}=0$, $\chi_{\boldsymbol{q}}^{\nu\mu}=\chi_0^{\nu\mu}/[1+(\xi_\chi^{\nu\mu})^2 q^2]$ $(\nu\mu=+-,zz)$. We obtain

$$\xi_\chi^{+-}=\sqrt{\alpha_1^{+-}\langle S^z\rangle/h}, \tag{46}$$

and

$$\xi_\chi^{zz}=\sqrt{2\alpha_1^{zz}C_{10}^{(0)-+}/\Delta^{zz}}. \tag{47}$$

Deriving Eq. (46) the regularity condition [Eq. (17)] for $n=0$, which reads as $h\langle S^z\rangle=zC_{10}g_0$, and Eq. (16), yielding the relation $\Delta^{+-}=2h(C_{10}/\langle S^z\rangle-\alpha_1^{+-}\langle S^z\rangle)$, have been used. Let us point out that the correlation lengths $\xi_\chi^{\nu\mu}$ generally deviate from $\xi^{\nu\mu}$ defined by Eqs. (44) and (45).

First, we consider the correlation length in zero field, where $\xi^{+-}=\xi^{zz}\equiv\xi$. In one dimension, the low-temperature expansion yields $\lim_{T\to 0}\xi T=S^2$ (Ref. 19), which agrees with the MSWT result[33] and, for $S=1/2$, with the result obtained by the thermal Bethe-ansatz method of Ref. 38. The renormalization-group approach of Ref. 35 combined with QMC simulations yields $\lim_{T\to 0}\xi T=1.14S^2$. In Fig. 8, the zero-field correlation length of the 1D ferromagnet is shown. Let us stress the very good agreement of our QMC data for $S=1/2$ with the Bethe-ansatz results of Ref. 38. Even on the finer scale of the inset, deviations are almost invisible. For comparison, also the QMC data of Ref. 35 and a one-parameter fit are given in the inset. Moreover, we obtain a good agreement of the Green-function theory, where ξ is calculated from definition (44), with our QMC data. In addition to ξ, in Fig. 8, the correlation length ξ_χ that is calculated for $S=1/2$ and $S=1$ by Eq. (47) $[\alpha_1^{zz}=\alpha,\ C_{10}^{(0)-+}=C_{10},\ \Delta^{zz}=\Delta$ given by Eq. (39)] is plotted. For $T\lesssim 0.25$, i.e., $\xi>1$, ξ_χ nearly coincides with ξ. With increasing temperature, i.e., with decreasing $\xi<1$, the deviation of ξ_χ from ξ appreciably increases. In the high-temperature limit, we get $\xi_\chi^{-1}=\{3T/S(S+1)\}^{1/2}$ resulting from $C_{10}=2[S(S+1)]^2/9\ T$ (Ref. 19). In the following, we plot ξ_χ in such cases only, where ξ_χ remarkably deviates from ξ.

In two dimensions, the zero-field correlation length in the second-order Green-function theory exponentially increases for $T\to 0$, $\xi\propto\exp(\pi S^2/T)$ (Ref. 19). As is the case for the magnetic susceptibility, the exponent is smaller by a factor of 2 compared to the MSWT[33] and the renormalization-group approach.[36]

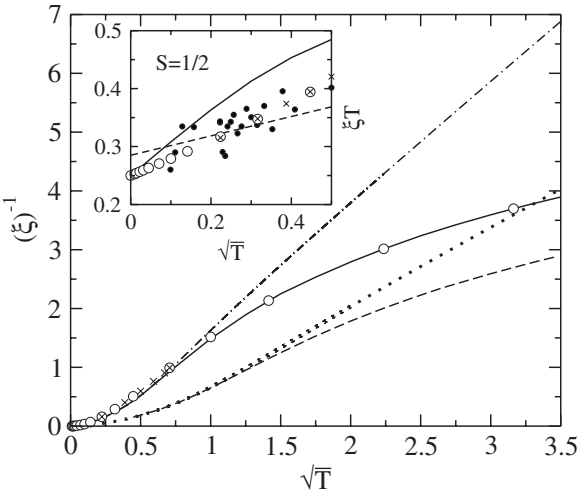

FIG. 8. Zero-field correlation length of the 1D ferromagnet with $S=1/2$ that is obtained by the Green-function theory (solid lines) and by the QMC simulations (×, $L=32$) and with $S=1$ resulting from the theory (long-dashed line). For comparison, the correlation length ξ_χ that is determined from the expansion of the static susceptibility around $\boldsymbol{q}=0$ is plotted for $S=1/2$ (dotted-dashed line) and $S=1$ (dotted line). The results for $S=1/2$ are compared to the Bethe-ansatz data of Ref. 38 (○) and with the QMC data of Ref. 35 (●) depicted in the inset together with a one-parameter fit (short-dashed line).

For $h\neq 0$, the transverse and longitudinal correlation lengths qualitatively reveal different temperature dependences. By considering the transverse correlation length ξ^{+-}, as shown in Fig. 9, the magnetic field cuts off the divergence of the zero-field correlation length at $T=0$, which corresponds to the absence of a phase transition and is evident from Eq. (46), $\xi_\chi^{+-}(T=0)=\sqrt{S/h}$ agreeing with the RPA result [Eq. (A4)] derived in the Appendix. As can be seen in the inset of Fig. 9(a) in the 1D $S=1/2$ model, we obtain good agreement of our analytical results for $T=0.4$ and $h\leqslant 1.2$ with the Bethe-ansatz data of Ref. 39. However, the comparison of the theory to the available Bethe data for $T=0.4$ and fields up to $h=4$ and for $T=0.2$ (Ref. 39) is hampered by numerical uncertainties, resulting from too small values of Δ^{+-}. Note the remarkably good agreement of ξ^{+-} with the RPA results (see inset). Concerning the dimensional dependence, in contrast to the case $h=0$, ξ^{+-} in one and two dimensions qualitatively exhibits the same behavior as $T\to 0$. In the 2D model [Fig. 9(b)], the deviation of ξ_χ^{+-} from ξ^{+-} increases with decreasing temperature, i.e., with increasing $\xi^{+-}>1$, which is clearly seen at $h=0.01$ and is opposite to the behavior in the $h=0$ case.

In Fig. 10, the longitudinal correlation length of the 1D ferromagnet is shown, where the QMC data are found to be in a fair agreement with our theory. This refers, in particular, to the $S=1/2$ model, where our results that are obtained by the simplified approach of Ref. 18 are plotted as well. Considering $h=0.05$ at low temperatures, those results remarkably deviate from the QMC data and our extended theory with $\alpha_2^{\nu\mu}\neq\alpha_1^{\nu\mu}$. In contrast to ξ^{+-}, the behavior of ξ^{zz} as $T\to 0$ is not conclusive, which is due to numerical uncertainties at low temperatures, where the long-distance correlators

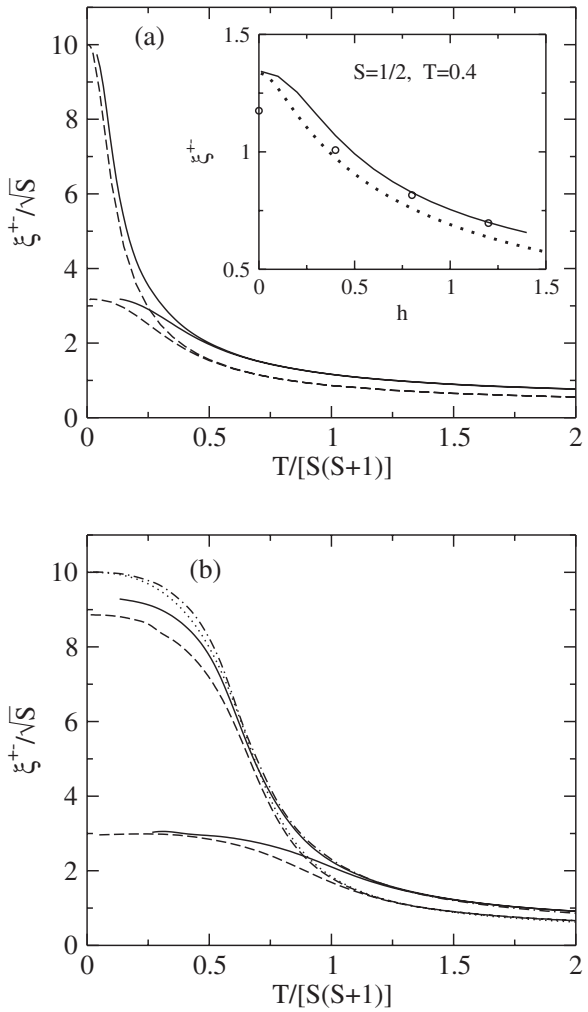

FIG. 9. Transverse correlation length of the (a) 1D and (b) 2D ferromagnets with $S=1/2$ (solid lines) and $S=1$ (dashed lines) in the fields $h=0.01$ and 0.1, from top to bottom. In the 2D case at $h=0.01$, the correlation length ξ_χ^{+-} that is calculated from the static susceptibility is shown for $S=1/2$ (dotted-dashed line) and $S=1$ (dotted line). In the inset the results of the Green-function theory are compared to the Bethe-ansatz data of Ref. 39 (○) and the RPA (dotted line).

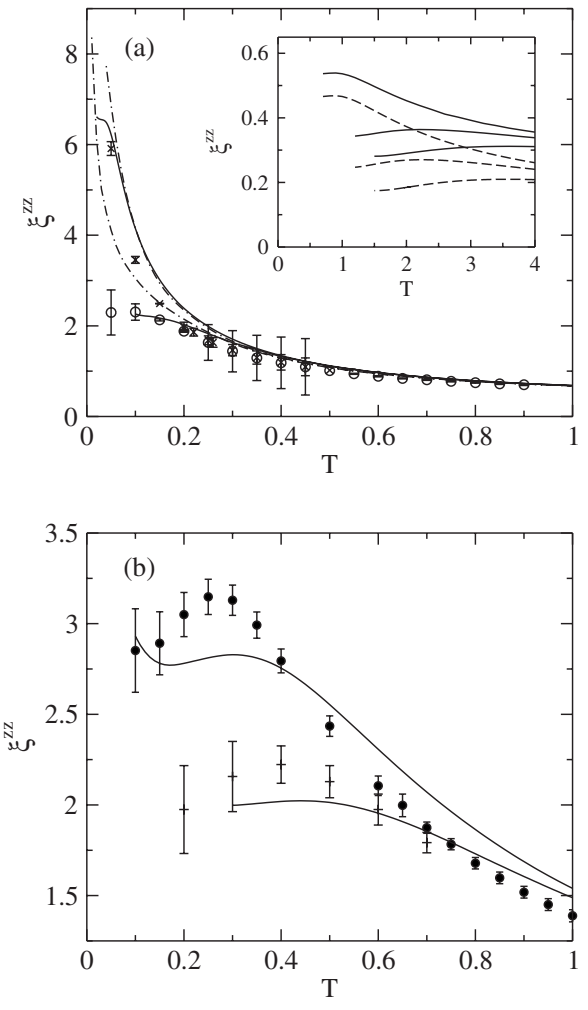

FIG. 10. Longitudinal correlation length of the 1D ferromagnet with (a) $S=1/2$ and (b) $S=1$ in the fields (a) $h=0.005$ and 0.05 and (b) $h=0.05$ and 0.1, from top to bottom, which is calculated by the Green-function (solid lines) and by the QMC methods (×, ○; $L=32$ and ●, +; $L=32$) and, for $S=1/2$, by the method of Ref. 18 (dotted-dashed lines). The inset exhibits the results for $S=1/2$ at the strong fields $h=1$, 3, and 5, from top to bottom, in comparison to the correlation length ξ_χ^{zz} (dashed lines) that is obtained from the static susceptibility.

$\bar{C}_{\boldsymbol{R}}^{(0)zz}$ needed to calculate ξ^{zz} are very small. For example, for $S=1/2$ and strong fields [see inset of Fig. 10(a)], the relevant correlators in the temperature region, where results are not given, are smaller than about 10^{-10}–10^{-14}. Moreover, for $S=1$, the results of the theory are reliable only at $T>T_0\simeq 0.1$ and 0.3 for $h=0.05$ and 0.1, respectively [see Fig. 10(b)]. At $T<T_0$, the relevant correlators, being smaller than about 10^{-4}, reveal an unreasonable behavior. This may be ascribed to our choice of a closed system of self-consistency equations for $S>1/2$, as described in Sec. II. Whereas the relative deviation of the NN correlators $C_{10}^{(0)zz}$ resulting from the self-consistency equations and from Eq. (31) is small (see Sec. II), the corresponding deviation of the correlators $\bar{C}_{10}^{(0)zz}$ becomes very large at low temperatures. Depending on the field and spin, the temperature dependence of ξ^{zz} in the 1D ferromagnet reveals a maximum at $T_m^\xi>0$. This anomaly can be clearly seen in the 1D $S=1$ model at low fields [Fig. 10(b)]. On the other hand, in the 1D $S=1/2$ model, the maximum appears at high fields, $h>0.8$ [see inset of Fig. 10(a)]. Moreover, as can be seen from Fig. 10, keeping the field $h=0.05$ fixed, the maximum develops with increasing spin. Note that a maximum of ξ^{zz} at a finite temperature is not obtained by the approach of Ref. 18. To our knowledge, such an anomaly in the correlation length has not been found before. To get some insight into the maximum of ξ^{zz}, we first suggest that larger correlation lengths may be connected with larger correlation functions. Correspondingly, we consider the maximum of $\bar{C}_{\boldsymbol{R}}^{(0)zz}$ at $T_m^{zz}(R)$, where $T_m^{zz}(R)>T_m^\xi$. By a detailed analysis, we find $T_m^{zz}(R)$ in the limit $R\to\infty$ to coincide with T_m^ξ in all cases, where ξ^{zz} has a maximum at $T_m^\xi>0$ (see Fig. 10), i.e., $\lim_{R\to\infty} T_m^{zz}(R)=T_m^\xi$. This result is corroborated by the conditions for a maximum which may be derived from ansatz (45). We get $\frac{1}{R}\partial \ln \bar{C}_{\boldsymbol{R}}^{(0)zz}/\partial T$

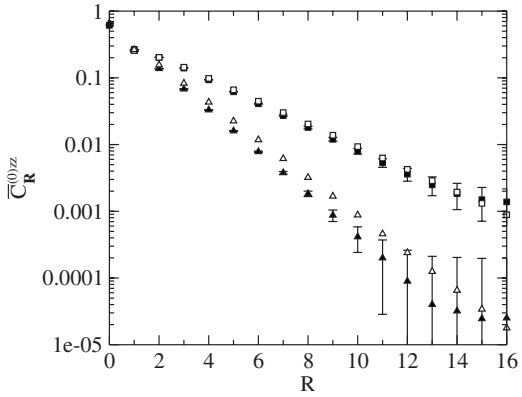

FIG. 11. Correlation function $\bar{C}_{\boldsymbol{R}}^{(0)zz}=\langle S_0^z S_{\boldsymbol{R}}^z\rangle-\langle S^z\rangle^2$ vs $R=|\boldsymbol{R}|$ for the 1D $S=1$ ferromagnet in the field $h=0.05$ at $T=0.5$ and 1.0, from top to bottom, which is calculated by the Green-function theory (open symbols) and by the QMC (filled symbols, $L=32$).

$=\frac{1}{R}\partial \ln A^{zz}/\partial T+\frac{1}{\xi}\partial \ln \xi/\partial T$. At $T_m^{zz}(R)$, we have $\frac{1}{\xi}\partial \ln \xi/\partial T=-\frac{1}{R}\partial \ln A^{zz}/\partial T$ and, for $R\to\infty$, $\partial\xi/\partial T=0$. As can be easily verified, the maximum condition $\partial^2\bar{C}_{\boldsymbol{R}}^{(0)zz}/\partial T^2<0$ results in $\partial^2\xi^{zz}/\partial T^2<0$. To compare the QMC and Green-function methods yielding the anomaly of ξ^{zz} in the 1D $S=1$ model [Fig. 10(b)] in more detail, in Fig. 11, the distance dependence of the corresponding correlator $\bar{C}_{\boldsymbol{R}}^{(0)zz}$ at $h=0.05$ is depicted. For $T=0.5$, a very good agreement of both methods is found.

In two dimensions, the anomaly of ξ^{zz} in the $S=1/2$ ferromagnet is more pronounced than in the 1D system and already appears at low fields, as can be seen in Fig. 12. In contrast to the 1D case, both the QMC data and the Green-function theory clearly reveal a minimum in addition to the maximum. Note that the statistical QMC errors in the interesting temperature region are smaller than the size of the symbols. Figure 12 demonstrates the qualitative effects of our extended theory ($\alpha_2^{\nu\mu}\neq\alpha_1^{\nu\mu}$) on the temperature dependence of ξ^{zz} compared to the simplified approach ($\alpha_2^{\nu\mu}=\alpha_1^{\nu\mu}$). Whereas this approach yields a slightly better agreement of the magnetization with the QMC data (see inset), it fails to describe the minimum-maximum anomaly.

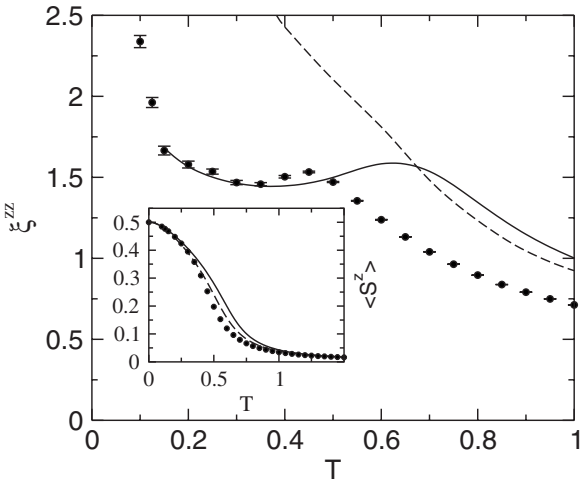

FIG. 12. Longitudinal correlation length of the 2D $S=1/2$ ferromagnet at $h=0.05$ that is calculated by the Green-function theory (solid lines), by the QMC simulations (●, $L=16$), and by the method of Ref. 18 (dashed lines). In the inset, the corresponding magnetization is plotted.

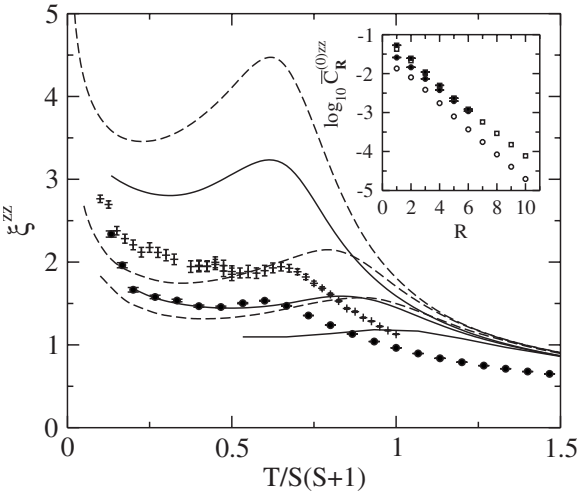

FIG. 13. Longitudinal correlation length of the 2D ferromagnet with $S=1/2$ (solid lines) and $S=1$ (dashed lines) in the fields $h=0.01$, 0.05, and 0.10, from top to bottom, compared to the QMC results at $h=0.05$ for $S=1/2$ (●, $L=16$) and $S=1$ (+, $L=16$). The inset shows the correlation function $\bar{C}_{\boldsymbol{R}}^{(0)zz}=\langle S_0^z S_{\boldsymbol{R}}^z\rangle-\langle S^z\rangle^2$ vs $R=|\boldsymbol{R}|$ for the 2D $S=1/2$ ferromagnet in the field $h=0.05$ at $T=0.4$ and 0.6, from bottom to top, which is calculated by the Green-function theory (open symbols) and by the QMC (filled symbols, $L=16$).

Figure 13 shows the field and spin dependence of the temperature behavior of ξ^{zz} in the 2D ferromagnet. As results from the theory, the anomaly of ξ^{zz} becomes more pronounced with decreasing field and with increasing spin. Let us point out that our QMC data for $h=0.05$ yield a minimum and a maximum of ξ^{zz} for both the $S=1/2$ and $S=1$ models and give confidence in the results of the theory. As in the 1D model, the maximum of ξ^{zz} at T_m^{ξ} is related to the maximum of $\bar{C}_{\boldsymbol{R}}^{(0)zz}$ by $\lim_{R\to\infty}T_m^{zz}(R)=T_m^{\xi}$ in all case, as shown in Fig. 13. The minimum of ξ^{zz} results from the different temperature dependences of $\bar{C}_{\boldsymbol{R}}^{(0)zz}$ and A^{zz} in ansatz (45). In analogy to Fig. 11, for a more detailed comparison, the inset exhibits the correlator $\bar{C}_{\boldsymbol{R}}^{(0)zz}$ for $S=1/2$ and $h=0.05$ as a function of the distance. The relative magnitude of the correlators at $T=0.4$ and 0.6 may be understood by the maximum in the temperature dependence of $\bar{C}_{\boldsymbol{R}}^{(0)zz}$.

C. Specific heat

Let us first consider the NN spin correlation functions $C_{10}^{(0)-+}$ and $C_{10}^{(0)zz}$ entering the internal energy $u=-z/2(C_{10}^{(0)-+}+C_{10}^{(0)zz})-h\langle S^z\rangle$. As an example, for the 1D $S=1$ model, they are depicted in Fig. 14, where we obtain a very good agreement of the analytical results with the QMC data. On the contrary, the RPA results for $C_{10}^{(0)-+}$ remarkably exceed the QMC data, and for $C_{10}^{(0)zz}$, the RPA yields negative values being incompatible with the ferromagnetic SRO.

In Fig. 15, the specific heat $C=\partial u/\partial T$ for the 1D $S=1/2$ ferromagnet at low fields is plotted. Again, our QMC data

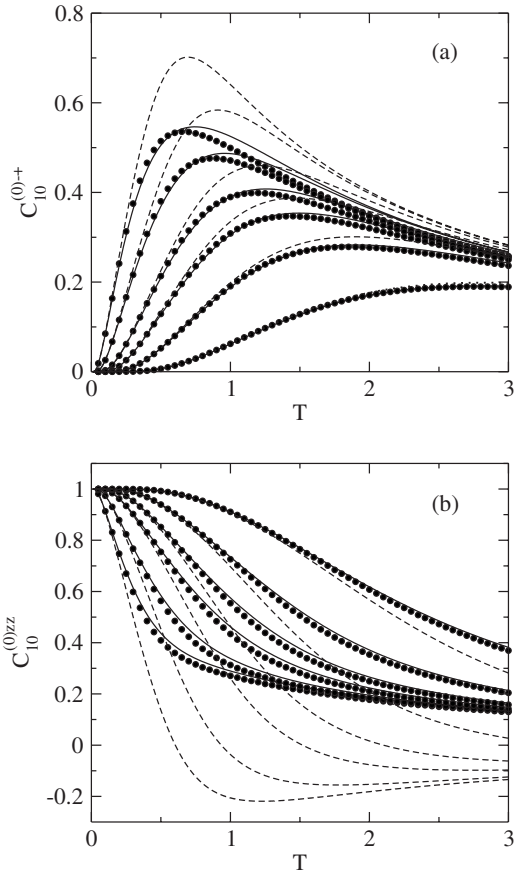

FIG. 14. (a) Transverse and (b) longitudinal nearest-neighbor two-spin correlation functions of the 1D $S=1$ ferromagnet at the fields $h=0.1$, 0.2, 0.4, 0.6, 1.0, and 2.0, from left to right, which are obtained by the Green-function theory (solid lines), by the QMC (●, $L=64$), and by the RPA (dashed lines).

agree very well with the Bethe-ansatz results.[17] At very low magnetic fields, the low-temperature maximum appearing, in the exact approaches at $h \lesssim 0.008$, in addition to the high-temperature maximum is much better described by the

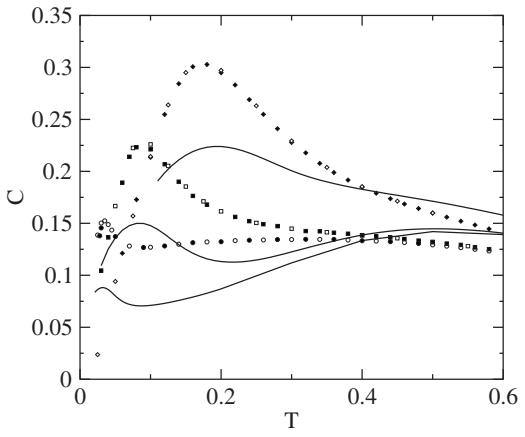

FIG. 15. Specific heat of the 1D $S=1/2$ ferromagnet that is obtained by the Green-function (solid lines) and by the QMC (filled symbols, $L=128$) methods at low fields, $h=0.005$, 0.03, and 0.1, from bottom to top, and compared to the Bethe-ansatz data of Ref. 17 (open symbols).

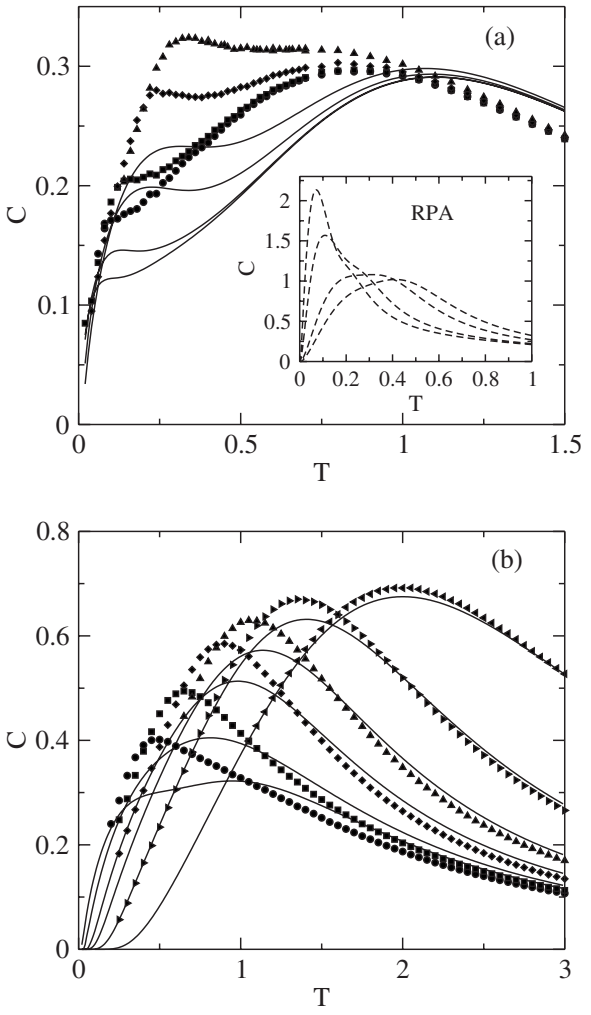

FIG. 16. Specific heat of the 1D $S=1$ ferromagnet that is obtained by the Green-function theory (solid lines) (a) at low fields, $h=0.005$, 0.01, 0.03, and 0.05, from bottom to top, with the QMC results for $L=64$ (filled symbols) and (b) at higher fields, $h=0.1$, 0.2, 0.4, 0.6, 1.0, and 2.0, from left to right, in comparison to the QMC results for $L=64$ (filled symbols). The inset shows the RPA data at the fields given in (a), from top to bottom, at $T=0.1$.

theory than we have found in Ref. 17. In our Green-function theory, this maximum appears up to higher fields, $h \leqslant 0.071$, and the deviation of the maximum position $T_{m,1}^C$ from the Bethe-ansatz and QMC values in the region $0.001 \leqslant h \leqslant 0.01$ is less than 8%. By considering very low fields, $h=0.001-0.01$ in steps of 0.001, $T_{m,1}^C$ and height $C(T_{m,1}^C)$ are fitted by using the following power laws:

$$T_{m,1}^C = 0.462h^{0.501}, \quad C(T_{m,1}^C) = 0.394h^{0.282}. \tag{48}$$

The exponents are in good agreement with the values of the Bethe-ansatz results,[17] $T_{m,1}^C=0.596h^{0.542}$ and $C(T_{m,1}^C)=0.513h^{0.228}$. Note that the specific heat in the 2D model has only one maximum.[17]

Figure 16 displays the specific heat of the 1D $S=1$ ferromagnet. At low magnetic fields, $0.007 \lesssim h \lesssim 0.057$, besides the high-temperature maximum, a low-temperature maximum appears [see Fig. 16(a)]. The position $T_{m,1}^C$ of this maxi-

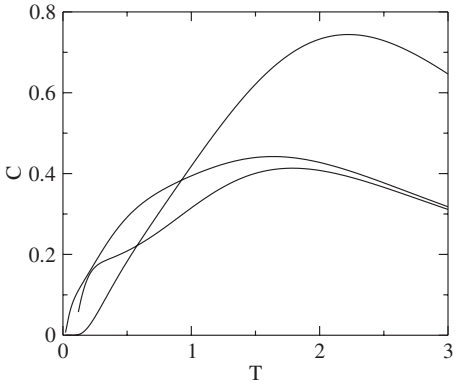

FIG. 17. Specific heat of the 1D $S=3/2$ ferromagnet that is calculated by the Green-function theory at $h=0.01$, 0.1, and 1.0, from bottom to top (at $T=1.5$).

mum that is obtained by the Green-function theory nearly agrees with the QMC results. As in the $S=1/2$ case,[17] in RPA a double maximum is not obtained [see inset of Fig. 16(a)], and the values of the specific heat maximum are much higher than the QMC values, which is ascribed to a poor description of SRO in RPA (see also Fig. 14). The specific heat of the 1D $S=3/2$ ferromagnet is shown in Fig. 17. There is no low-temperature maximum, but only a hump at low enough fields. For higher spins qualitatively the same behavior is found. The specific heat for the 2D $S=1$ ferromagnet is plotted in Fig. 18. As in the case $S=1/2$,[17] in two dimensions, only one maximum appears. At small fields, the position of the maximum in the Green-function theory is remarkably shifted to higher temperatures compared to the QMC data. Note that the RPA curves at low fields (see upper inset of Fig. 18) exhibit a too large maximum height, as was also found in the 1D model [inset of Fig. 16(a)].

From our investigations of the maximum behavior of the specific heat in dependence on spin and dimension, we conclude that the appearance of two maxima is a distinctive effect of quantum fluctuations, which decrease with increasing spin and dimension. Note that in ferromagnets quantum fluctuations occur at nonzero temperatures only, whereas in antiferromagnets, they are important already at $T=0$. The characterization of the occurrence of two maxima in the temperature dependence of the specific heat of the Heisenberg ferromagnet as a peculiar quantum effect is corroborated by recent QMC simulations of the 1D classical Heisenberg model and the 1D $S=1/2$ Ising model in a magnetic field,[40] where only one maximum in the specific heat was found.

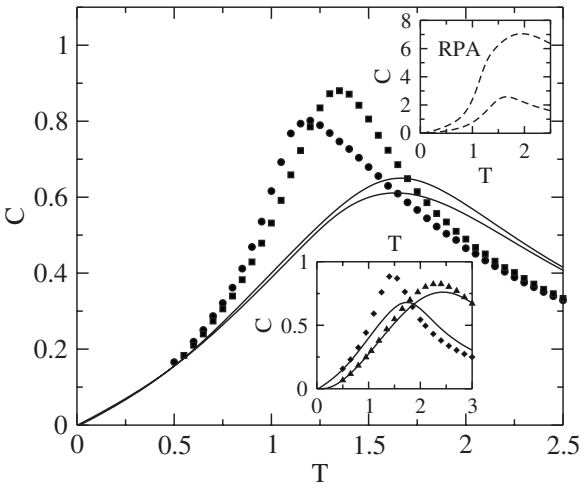

FIG. 18. Specific heat of the 2D $S=1$ ferromagnet at $h=0.01$ and 0.05, from bottom to top, and, as depicted in the lower inset, at $h=0.1$ and 1.0, from left to right, where the Green-function (solid lines) and QMC (filled symbols, $L=64$) results are shown. In the upper inset, the RPA results for $h=0.01$ and 0.05, from top to bottom, are plotted.

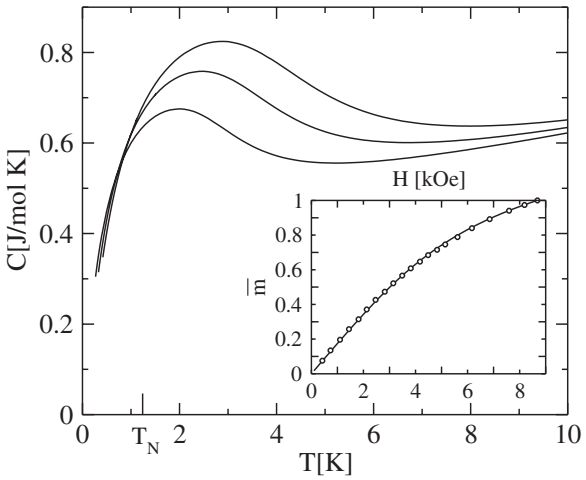

FIG. 19. Specific heat of the copper salt TMCuC (Refs. 2 and 3, Néel temperature $T_N=1.24$ K), as predicted by the theory for the $S=1/2$ 1D ferromagnet in the magnetic fields $H=2$, 3, and 4 kOe, from bottom to top, with $J=6.18$ meV obtained from the fit of the reduced magnetization $\bar{m}=m(H)/m(H=8.7\ \text{kOe})$ at $T=4.1$ K to experimental data (○) shown in the inset.

D. Comparison to experiments

Let us compare our results to experiments on $S=1/2$ quasi-1D ferromagnets, where we focus on the possible observation of two maxima in the temperature dependence of the specific heat as a characteristic feature of 1D ferromagnets in a magnetic field.

The copper salt TMCuC $[(CH_3)_4NCuCl_3]$ was shown[2,3] to be a good 1D Heisenberg ferromagnet, which is reflected in the small value of the Néel temperature $T_N=1.24$ K for 3D ordering.[3] Determining the exchange energy J by a least-squares fit of the theory for $S=1/2$ to the experimental data for the magnetization as a function of the magnetic field H at $T=4.1$ K,[2] we obtain $J=6.18$ meV and a very good agreement with experiments, as can be seen in the inset of Fig. 19. Note that the value of J lies between the values given in Ref. 2 ($J=5.17$ meV) and in Ref. 3 ($J=7.76$ meV). According to the QMC and Bethe-ansatz results for the 1D $S=1/2$ ferromagnet, two maxima of the specific heat occur for $h \lesssim 0.008$ or using the relation $h=1.16 \times 10^{-2} H\ (\text{kOe})/J\ (\text{meV})$ for $H \leqslant 4$ kOe. In Fig. 19, the specific heat, as predicted by the theory using the fit value of J, is plotted. The low-temperature maximum for $H=2$, 3, and 4 kOe occurs at $T^C_{m,1}=2.0$, 2.5, and 2.9 K, respectively. The

high-temperature maximum (not shown in Fig. 19) appears at about $T^C_{m,2}=37.4$ K with $C(T^C_{m,2})=1.18$ J/mol K for all fields considered. In the quasi-1D system, the anomaly of the specific heat at T_N, which cannot be described by our theory for a purely 1D system, may mask the low-temperature maximum if $T^C_{m,1}$ is not sufficiently larger than T_N. At $H=3$ kOe (4 kOe), we have $T^C_{m,1}/T_N=2.0$ (2.3). From this, we predict that in TMCuC above T_N two maxima in the specific heat at moderate magnetic fields, $H=3-4$ kOe, may be observed.

Considering the quasi-1D organic ferromagnet *p*-NPNN ($C_{13}H_{16}N_3O_4$) in the γ phase with $J=0.37$ meV,[4,5] where the phase transition at $T_N=0.65$ K for $H=0$ persists up to $H=1.8$ kOe ($T_N\simeq 0.5$ K), two maxima of the specific heat above T_N cannot be observed because at $h\lesssim 0.008$ ($H\lesssim 0.26$ kOe), we have $T^C_{m,1}\lesssim 0.19$ K $<T_N$. The analogous situation, in which the low-temperature maximum in the specific heat of the 1D ferromagnet cannot be seen, is found for the following compounds. Considering the ferromagnetic chains in the quasi-1D magnet β-BBDTA·$GaBr_4$ with $J=0.375$ meV,[6] we have $T^C_{m,1}\lesssim 0.19$ K, which is lower than the temperature of the specific-heat cusp, $T_C\geqslant 0.4$ K, caused by the interchain coupling. For the $CuCl_2$-tetramethylsulfoxide (dimethylsulfoxide) salts with $J=3.36$ (3.88) meV,[7] we get $T^C_{m,1}\lesssim 1.7$ (1.96) K being lower than the temperature of the susceptibility maximum, 3.9 (5.4) K, indicating the influence of the antiferromagnetic interchain coupling.

V. SUMMARY

In this paper, we have developed a second-order Green-function theory for the 1D and 2D Heisenberg ferromagnets in a magnetic field, which extends our previous approach[17] to arbitrary spins and by the calculation of the correlation length. In addition, we have performed QMC simulations of the $S=1/2$ and $S=1$ models on a chain up to $N=1024$ sites and on a square lattice up to $N=64\times 64$ by using the stochastic series expansion method with directed loop updates. The approximate analytical and quasiexact numerical results turned out to be in good agreement, in particular, for the ferromagnetic quantum spin chains. Analyzing the field dependence of the maximum in the temperature dependence of the magnetic susceptibility over a much broader field region as previously considered,[17] we have found power laws for the position and height of the susceptibility maximum. The transverse and longitudinal correlation lengths were shown to have qualitatively different temperature dependences. Depending on spin, field, and dimension, the longitudinal correlation length ξ^{zz} reveals an unexpected anomaly: with increasing temperature, ξ^{zz} exhibits a minimum followed by a maximum. By a detailed investigation of the specific heat of the Heisenberg chain with arbitrary spin, two maxima in its temperature dependence at low magnetic fields were detected for $S=1/2$ and $S=1$, whereas for $S>1$, only one maximum appears, as in the 2D case. The existence of two specific-heat maxima was identified as a distinctive quantum effect. The theory was compared to magnetization experiments on the 1D copper salt TMCuC, and predictions for the temperature dependence of the specific heat, in particular, for the occurrence of two maxima, were made, which should be measurable experimentally.

ACKNOWLEDGMENTS

The authors wish to thank J. Richter, N. M. Plakida, and S. Wenzel for valuable discussions. This work was partially supported (L.B. and W.J.) by the EU through the Marie Curie Host Development under Grant No. IHP-HPMD-CT-2001-00108 and by the supercomputer time Grant No. hlz12 of the John von Neumann Institute for Computing (NIC), Forschungszentrum Jülich.

APPENDIX: RANDOM-PHASE APPROXIMATION

It is of interest to compare our results for finite magnetic fields with the RPA.[16] Considering the equation of motion [Eq. (2)], the Tyablikov decoupling $iS^+_{\boldsymbol{q}}=\omega_{\boldsymbol{q}}S^+_{\boldsymbol{q}}$ yields

$$\langle\langle S^+_{\boldsymbol{q}};S^{(n)-}_{-\boldsymbol{q}}\rangle\rangle_\omega=\frac{M^{(n)+-}}{\omega-\omega_{\boldsymbol{q}}},\quad \omega_{\boldsymbol{q}}=z\langle S^z\rangle(1-\gamma_{\boldsymbol{q}})+h, \tag{A1}$$

with $M^{(n)+-}$ given by Eq. (4). By comparing the correlation function $\langle(S^z_i)^nS^-_iS^+_i\rangle$ resulting from Eq. (A1) with the expression that is obtained by Eq. (6) multiplied by $(S^z_i)^n$ and by using the identity $\Pi^S_{m=-S}(S^z_i-m)=0$, $\langle S^z\rangle$ is obtained as[16]

$$\langle S^z\rangle=\{(S-P)(1+P)^{2S+1}+(1+S+P)P^{2S+1}\}\{(1+P)^{2S+1}-P^{2S+1}\}^{-1}, \tag{A2}$$

where $P=(1/N)\Sigma_{\boldsymbol{q}}n(\omega_{\boldsymbol{q}})$. The transverse two-spin correlation functions $C^{(0)-+}_{\boldsymbol{R}}$ are calculated from Eq. (A1) for $n=0$, which yields

$$C^{(0)-+}_{\boldsymbol{R}}=\frac{2\langle S^z\rangle}{N}\sum_{\boldsymbol{q}}n(\omega_{\boldsymbol{q}})e^{i\boldsymbol{qR}}. \tag{A3}$$

The transverse correlation length ξ^{+-} is calculated from the long-distance behavior of Eq. (A3) according to Eq. (44). For comparison, the correlation length ξ^{+-}_χ may be obtained from the expansion of the static spin susceptibility $\chi^{+-}_{\boldsymbol{q}}$ around $\boldsymbol{q}=0$ (cf. Sec. IV B). We get

$$\xi^{+-}_\chi=\sqrt{\frac{\langle S^z\rangle}{h}}. \tag{A4}$$

The longitudinal correlation functions $C^{(0)zz}_{\boldsymbol{R}\neq 0}$ cannot be obtained by the RPA, except for the NN correlation function $C^{(0)zz}_{10}$, which we evaluate proceeding as in Ref. 17 for $S=1/2$. That is, we calculate the internal energy in RPA starting from the exact representation [Eq. (23)] and inserting the RPA results [Eqs. (A1) and (A2)], $C^{(1)-+}_{10}=(1/N)M^{(1)+-}\Sigma_{\boldsymbol{q}}n(\omega_{\boldsymbol{q}})\cos q_x$, with $M^{(1)+-}=3\langle(S^z)^2\rangle-\langle S^z\rangle-S(S+1)$ and $\langle(S^z)^2\rangle=S(S+1)-\langle S^z\rangle(1+2P)$, resulting from Eq. (6). Moreover, we perform the decoupling $C^{(1)zz}_{10}=\langle S^z\rangle\langle(S^z)^2\rangle$. From u, $C^{(0)-+}_{10}$, and $\langle S^z\rangle$, the correlator $C^{(0)zz}_{10}$ may be calculated.

[1] *Quantum Magnetism*, Lecture Notes in Physics Vol. 645, edited by U. Schollwöck, J. Richter, D. J. J. Farnell, and R. F. Bishop (Springer, Berlin, 2004).
[2] C. P. Landee and R. D. Willett, Phys. Rev. Lett. **43**, 463 (1979).
[3] C. Dupas, J. P. Renard, J. Seiden, and A. Cheikh-Rouhou, Phys. Rev. B **25**, 3261 (1982).
[4] M. Takahashi, P. Turek, Y. Nakazawa, M. Tamura, K. Nozawa, D. Shiomi, M. Ishikawa, and M. Kinoshita, Phys. Rev. Lett. **67**, 746 (1991); Y. Nakazawa, M. Tamura, N. Shirakawa, D. Shiomi, M. Takahashi, M. Kinoshita, and M. Ishikawa, Phys. Rev. B **46**, 8906 (1992).
[5] M. Takahashi, M. Kinoshita, and M. Ishikawa, J. Phys. Soc. Jpn. **61**, 3745 (1992).
[6] K. Shimizu, T. Gotohda, T. Matsushita, N. Wada, W. Fujita, K. Awaga, Y. Saiga, and D. S. Hirashima, Phys. Rev. B **74**, 172413 (2006).
[7] D. D. Swank, C. P. Landee, and R. D. Willett, Phys. Rev. B **20**, 2154 (1979).
[8] S. E. McLain, D. A. Tennant, J. F. C. Turner, T. Barnes, M. R. Dolgos, Th. Proffen, B. C. Sales, and R. I. Bewley, arXiv:cond-mat/0509194 (unpublished).
[9] W-H. Li, C. H. Perry, J. B. Sokoloff, V. Wagner, M. E. Chen, and G. Shirane, Phys. Rev. B **35**, 1891 (1987); S. Feldkemper, W. Weber, J. Schulenburg, and J. Richter, *ibid.* **52**, 313 (1995); H. Manaka, T. Koide, T. Shidara, and I. Yamada, *ibid.* **68**, 184412 (2003).
[10] G. Kamieniarz and C. Vanderzande, Phys. Rev. B **35**, R3341 (1987); G. M. Wysin and A. R. Bishop, *ibid.* **34**, 3377 (1986).
[11] P. Fröbrich, P. J. Jensen, and P. J. Kuntz, Eur. Phys. J. B **13**, 477 (2000); P. Fröbrich, P. J. Jensen, P. J. Kuntz, and A. Ecker, *ibid.* **18**, 579 (2000); P. Fröbrich and P. J. Kuntz, *ibid.* **32**, 445 (2003).
[12] P. Henelius, P. Fröbrich, P. J. Kuntz, C. Timm, and P. J. Jensen, Phys. Rev. B **66**, 094407 (2002).
[13] S. Schwieger, J. Kienert, and W. Nolting, Phys. Rev. B **71**, 024428 (2005); M. G. Pini, P. Politi, and R. L. Stamps, *ibid.* **72**, 014454 (2005).
[14] R. Sellmann, H. Fritzsche, H. Maletta, V. Leiner, and R. Siebrecht, Phys. Rev. B **64**, 054418 (2001); S. Pütter, H. F. Ding, Y. T. Millev, H. P. Oepen, and J. Kirschner, *ibid.* **64**, 092409 (2001).
[15] P. Fröbrich, P. J. Kuntz, and M. Saber, Ann. Phys. **11**, 387 (2002).
[16] S. V. Tyablikov, *Methods in the Quantum Theory of Magnetism* (Plenum, New York, 1967).
[17] I. Junger, D. Ihle, J. Richter, and A. Klümper, Phys. Rev. B **70**, 104419 (2004).
[18] T. N. Antsygina, M. I. Poltavskaya, I. I. Poltavsky, and K. A. Chishko, Phys. Rev. B **77**, 024407 (2008).
[19] F. Suzuki, N. Shibata, and C. Ishii, J. Phys. Soc. Jpn. **63**, 1539 (1994).
[20] I. J. Junger, D. Ihle, and J. Richter, Phys. Rev. B **72**, 064454 (2005).
[21] S. Winterfeldt and D. Ihle, Phys. Rev. B **56**, 5535 (1997); **59**, 6010 (1999).
[22] J. Kondo and K. Yamaji, Prog. Theor. Phys. **47**, 807 (1972); K. Yamaji and J. Kondo, Phys. Lett. **45A**, 317 (1973).
[23] H. Shimahara and S. Takada, J. Phys. Soc. Jpn. **60**, 2394 (1991); **61**, 989 (1992).
[24] D. Schmalfuß, J. Richter, and D. Ihle, Phys. Rev. B **70**, 184412 (2004); **72**, 224405 (2005).
[25] P. J. Jensen and F. Aguilera-Granja, Phys. Lett. A **269**, 158 (2000).
[26] K. Elk and W. Gasser, in *Die Methode der Greenschen Funktionen in der Festkörperphysik* (Akademie-Verlag, Berlin, 1979); W. Nolting, *Quantentheorie des Magnetismus* (B. G. Teubner, Stuttgart, 1986), Vol. 2.
[27] A. W. Sandvik and J. Kurkijärvi, Phys. Rev. B **43**, 5950 (1991).
[28] O. F. Syljuasen and A. W. Sandvik, Phys. Rev. E **66**, 046701 (2002).
[29] W. Janke, in *Computational Many-Particle Physics*, Lecture Notes in Physics Vol. 739, edited by H. Fehske, R. Schneider, and A. Weiße (Springer, Berlin, 2008), pp. 79–140.
[30] A. W. Sandvik, R. R. P. Singh, and D. K. Campbell, Phys. Rev. B **56**, 14510 (1997).
[31] B. Efron, *The Jackknife, The Bootstrap and Other Resampling Plans* (Society for Industrial and Applied Mathematics, Philadelphia, 1982).
[32] W. H. Press, S. A. Teukolsky, W. T. Vetterling, and B. P. Flannery, *Numerical Recipes in Fortran 77: The Art of Scientific Computing* (Cambridge University Press, Cambridge, 2001).
[33] M. Takahashi, Prog. Theor. Phys. Suppl. **87**, 233 (1986); Phys. Rev. Lett. **58**, 168 (1987).
[34] M. Yamada and M. Takahashi, J. Phys. Soc. Jpn. **55**, 2024 (1986).
[35] P. Kopietz, Phys. Rev. B **40**, 5194 (1989).
[36] P. Kopietz and S. Chakravarty, Phys. Rev. B **40**, 4858 (1989).
[37] A. Hu, Y. Chen, and L. Peng, Physica B **393**, 368 (2007).
[38] M. Yamada, J. Phys. Soc. Jpn. **59**, 848 (1990).
[39] M. Takahashi, Phys. Rev. B **44**, 12382 (1991).
[40] S. Wenzel (unpublished).